Chromatin insulator bodies are nuclear structures that form in response to osmotic stress and cell death

Todd Schoborg, Ryan Rickels, Josh Barrios, and Mariano Labrador

Department of Biochemistry and Cellular and Molecular Biology, University of Tennessee, Knoxville, TN 37996

Chromatin insulators assist in the formation of higher-order chromatin structures by mediating long-range contacts between distant genomic sites. It has been suggested that insulators accomplish this task by forming dense nuclear foci termed insulator bodies that result from the coalescence of multiple protein-bound insulators. However, these structures remain poorly understood, particularly the mechanisms triggering body formation and their role in nuclear function. In this paper, we show that insulator proteins undergo a dramatic and dynamic spatial reorganization into insulator bodies during osmostress and cell death in a high osmolarity glycerol–p38 mitogen-activated protein kinase–independent manner, leading to a large reduction in DNA-bound insulator proteins that rapidly repopulate chromatin as the bodies disassemble upon return to isotonicity. These bodies occupy distinct nuclear territories and contain a defined structural arrangement of insulator proteins. Our findings suggest insulator bodies are novel nuclear stress foci that can be used as a proxy to monitor the chromatin-bound state of insulator proteins and provide new insights into the effects of osmostress on nuclear and genome organization.

Introduction

Packaging DNA in the nucleus requires the formation of higher-order chromatin structures that function as both structural and functional regulators of the genome. Central to this process is the formation of long-range contacts between distant genomic sites, resulting in the formation of loop structures that establish physical, topological, and gene regulatory domains in addition to facilitating contacts between promoters and distant regulatory elements. Although several chromatin-binding proteins have been implicated in this process, chromatin insulators are of particular interest given their broad role in chromatin structure and nuclear function. Despite their initial characterization from transgenic assays in *Drosophila melanogaster* as enhancer and heterochromatin blockers, the in vivo function of these DNA elements more generally involves mediating long-range contacts. Seven insulator-binding proteins have been identified in *Drosophila*, including Su(Hw), CP190, BEAF-32, Mod(mdg4)67.2, dCTCF, GAF, and Zw5, with mammals containing only the CTCF orthologue (Schoborg and Labrador, 2010). In both taxa, these proteins bind to thousands of insulator sites scattered throughout the genome (Bushey et al., 2009; Cuddapah et al., 2009; Nègre et al., 2010) where they participate in a plethora of long-range contacts with enhancers, promoters, and other insulators, acting to both facilitate and repress transcription, maintain regions of histone modifications, and establish physical domains (Krivega and Dean, 2012; Van Bortle and Corces, 2012; Yang and Corces, 2012).

It has been suggested that insulators spatially accomplish these tasks through the formation of multiple chromatin loop structures, mediated by contacts between multiple insulator-bound proteins, which physically manifest themselves as insulator bodies (Labrador and Corces, 2002). *Drosophila* insulator bodies consist of 10–30 punctate nuclear signals corresponding to Su(Hw), CP190, Mod(mdg4)67.2, and dCTCF (Gerasimova and Corces, 1998; Gerasimova et al., 2000; Pai et al., 2004;

Correspondence to Mariano Labrador: labrador@utk.edu

R. Rickels's present address is Stowers Institute for Medical Research, Kansas City, MO 64110.

J. Barrios's present address is Dept. of Biological Sciences, Louisiana State University, Baton Rouge, LA 70803.

Abbreviations used in this paper: ChIP, chromatin immunoprecipitation; C_t, cycle threshold; DsRNA, double-stranded RNA; HOG, high osmolarity glycerol; PcG, Polycomb group; qPCR, quantitative PCR; SUMO, small ubiquitin-like modifier.

The Rockefeller University Press $30.00
J. Cell Biol. Vol. 202 No. 2 261–276
www.jcb.org/cgi/doi/10.1083/jcb.201304181

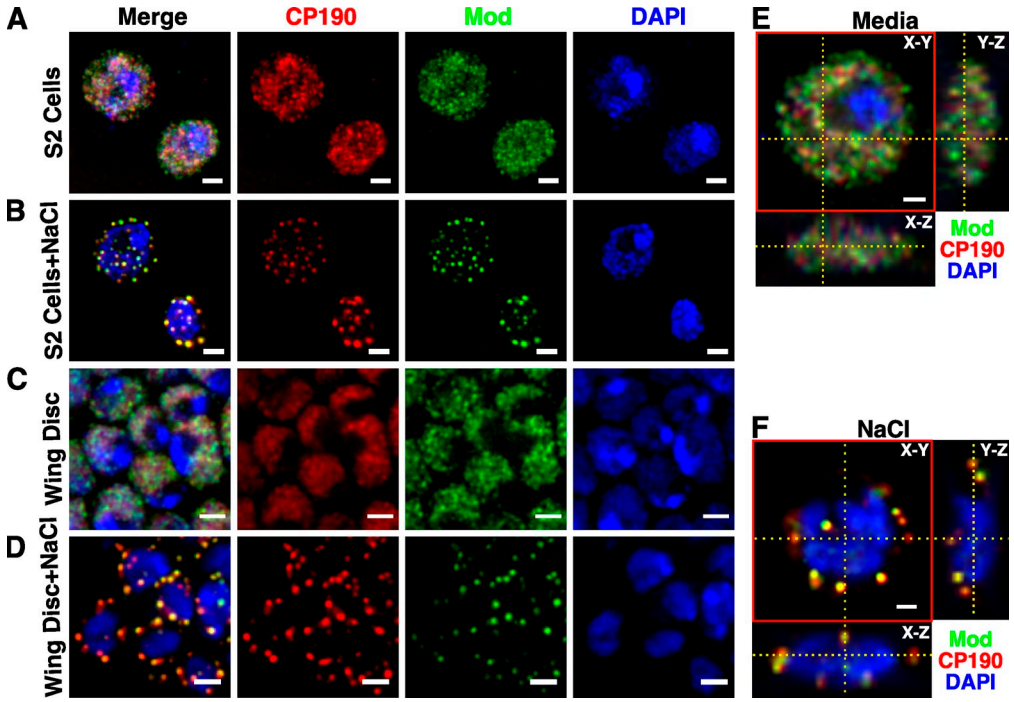

Figure 1. **Insulator bodies form in response to osmostress.** (A and B) S2 cells stained with CP190 and Mod(mdg4) under normal cellular conditions (A) or after treatment with 250 mM NaCl (B). (C and D) Wing discs from third instar larvae stained for CP190 and Mod(mdg4) under normal cellular conditions (C) or after treatment with 250 mM NaCl (D). (E and F) Orthogonal projections along the indicated axes (yellow dashed lines) in an unstressed (E) and stressed (F) S2 cell. The red box outlines the x-y plane image. Note that A–D are maximum projections of 1-µm z slices, whereas E and F are a single z slice (x-y plane only). Bars, 2 µm.

Gerasimova et al., 2007). Though early indirect evidence supported a functional role in *gypsy* insulator activity (Gerasimova et al., 2000; Byrd and Corces, 2003), recent work has suggested that these structures do not contribute to *gypsy* enhancer blocking directly and instead function as storage sites for insulator proteins poised for insulator activity (Golovnin et al., 2008, 2012). However, many fundamental aspects about these structures remain poorly understood, particularly how and why they form, whether they might contribute to other aspects of insulator function independently of enhancer blocking, and the consequences of such behavior on nuclear organization and genome dynamics.

Here, we show that insulator bodies are nuclear stress bodies that form in response to osmostress and cell death. Insulator proteins coalesce from diffusely distributed speckles into punctate insulator bodies rapidly in response to osmotic stress, exhibit dynamic behavior during the duration of stress, and rapidly recover to their prestressed state upon return to isotonicity. This correlates with a reduction in chromatin-bound insulator proteins during the duration of stress that is restored within minutes during recovery. Insulator bodies localize primarily to the nuclear periphery where they show transient associations with lamin, in addition to chromatin lacunas within the condensed chromatin mass. Interestingly, this behavior is independent of the high osmolarity glycerol (HOG)–p38 MAPK osmostress sensing pathway. In larval tissue, CP190 and Mod(mdg4)67.2 can form bodies independently of one another, whereas Mod(mdg4)67.2 is required for Su(Hw) entry into these structures. Our findings reveal novel insights into the role of stress on nuclear dynamics, provide a framework for elucidating the consequences of such behavior on genome function and organization, and establish a model system in which to study various aspects of nuclear body biogenesis, maintenance, and behavior.

Results

Insulator bodies form in response to hyperosmolarity

Previous work has primarily focused on insulator body behavior in third instar larval tissues and S2 cells (Gerasimova and Corces, 1998; Gerasimova et al., 2000, 2007; Ghosh et al., 2001; Pai et al., 2004; Xu et al., 2004; Capelson and Corces, 2005, 2006; Lei and Corces, 2006; Golovnin et al., 2008, 2012; Ramos et al., 2011; Wood et al., 2011). Using antibodies directed against CP190 and Mod(mdg4)67.2, we were unable to identify structures that resembled insulator bodies in these same cells and tissues (Figs. 1, A and C; and S1 B). Rather than exhibiting 10–30 nuclear periphery–associated punctate dots as observed in the aforementioned previous studies, our diploid cells displayed a diffuse distribution that appears speckled after image deconvolution. This pattern consists of numerous small foci, reminiscent of tiny speckles distributed throughout the entire volume of nucleus, with the exception of the nucleolus (Fig. 1 E). Both proteins formed distinct bands on polytene chromosomes as expected (see Figs. 7 A and S1 B). Occasionally, one or two small punctate dots resembling insulator bodies were observed for CP190 in larval tissue and S2 cells; however,

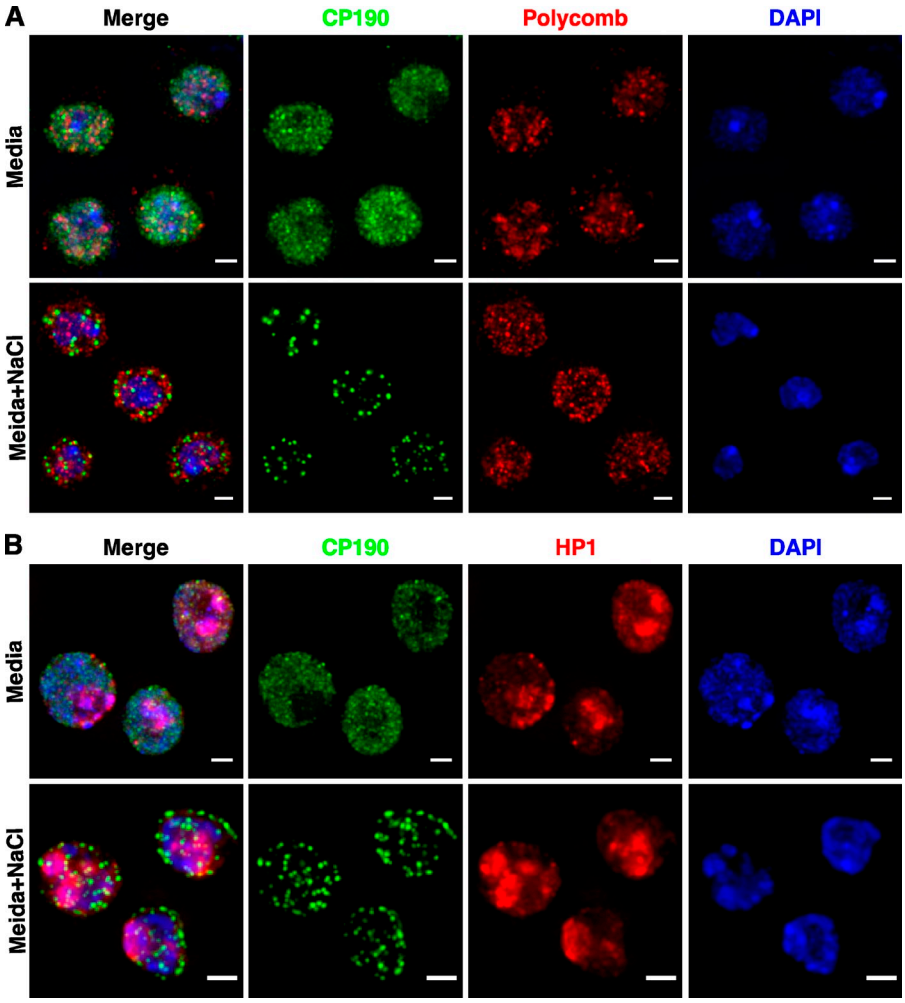

Figure 2. **Osmostress does not alter the nuclear distribution of other chromatin proteins.** (A and B) S2 cells treated with or without 250 mM NaCl and stained for CP190 and Polycomb (A) or HP1 (B). Bars, 2 µm.

the majority of the signal remained distributed throughout the nucleus (unpublished data).

Our inability to observe insulator bodies in cells and tissues under normal cellular conditions led us to next determine the effects of various stressors on insulator body formation. Previous work has implicated certain stress-induced cues as regulators of body behavior, particularly heat shock (Gerasimova et al., 2000; Wood et al., 2011; Golovnin et al., 2012). Treatment of S2 cells with a 37°C heat shock for 20 or 60 min did not change the distribution of CP190 and Mod(mdg4)67.2 compared with non–heat shock controls, despite an obvious rearrangement of chromatin in the heat-shocked cells (Fig. S1 A). However, subjecting cells and tissue to NaCl-induced osmotic stress resulted in the disruption of the diffusely speckled pattern and the formation of large CP190 and Mod(mdg4)67.2 foci in >99% of nuclei that was distinct from the unstressed control pattern, irrespective of cell/tissue type (Figs. 1, B, D, and F; and S1 B). These structures matched the description of insulator bodies given in previous studies at the beginning of this section, both in terms of number of bodies per nucleus and their localization to the nuclear periphery. Additionally, two chemically distinct osmolytes, sorbitol and sucrose, also induced body formation (Fig. S1 C). This appears to be a graded response, as CP190 gradually transitions from diffusely speckled to more punctate and numerous bodies as the salt concentration is increased up to 500 mM (Fig. S1 D). Cells permeabilized with detergent before addition of 250 mM NaCl failed to form bodies and instead maintained the diffusely speckled pattern observed in the absence of osmostress, verifying that insulator body formation occurs in response to increased osmotic loads (Fig. S1 E). Taken collectively, these data suggest that insulator bodies are novel nuclear stress bodies that form in response to osmostress.

Interestingly, this response appears to be relegated specifically to insulator proteins and their interacting partners. Other chromatin proteins, such as Polycomb group (PcG) proteins found in both *Drosophila* and mammals, have been shown to form speckle-like foci termed PcG bodies that may function as hubs involved in silencing developmental genes (Messmer et al., 1992; Alkema et al., 1997; Bantignies et al., 2011). PcG bodies in S2 cells marked with Polycomb are not significantly altered during osmostress, remaining identical in size and nuclear distribution as compared with untreated media controls, whereas CP190 undergoes a substantial reorganization into bodies (Fig. 2 A). Furthermore, HP1 (Heterochromatin Protein 1), which binds to H3K9 methylated histone tails primarily in heterochromatin (Vermaak and Malik, 2009), is not disrupted during osmostress (Fig. 2 B). Given the lack of a similar response by other nuclear proteins, these data suggest that insulator body

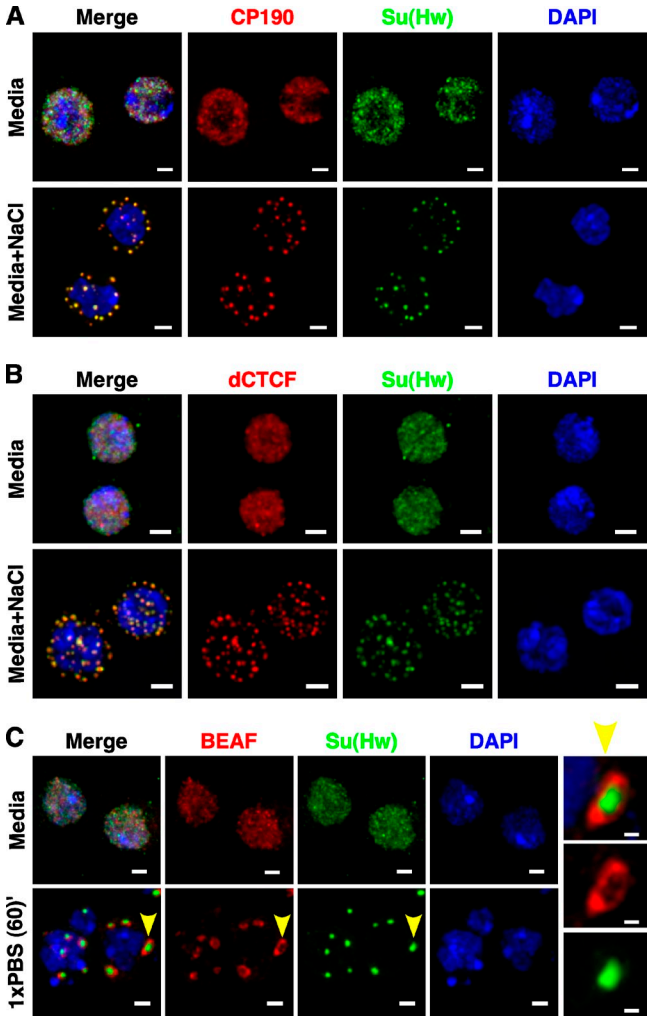

Figure 3. **Insulator bodies have a defined structural organization.** (A and B) S2 cells treated with or without 250 mM NaCl and stained for CP190 and Su(Hw) (A), dCTCF::mCherry and Su(Hw)::EGFP (B) and BEAF-32 and Su(Hw) after 60-min incubation in PBS. (C) BEAF-32 forms large donut structures around the spherical structures (arrowhead and insets). Bars: (A–C, main images) 2 µm; (C, insets) 0.5 µm.

formation is not the result of a general biophysical effect on globular protein structure under conditions of hyperosmolarity and instead may be the result of a targeted response directed to insulator proteins.

Insulator bodies are highly ordered structures with a distinct nuclear distribution

The location of known insulator proteins within these bodies suggests that they have a defined structural organization. We observed extensive colocalization between Su(Hw), Mod(mdg4)67.2, CP190, and dCTCF proteins in stressed nuclei, which manifest themselves as irregular spherical structures (Fig. 3, A and B) in agreement with previous studies (Gerasimova and Corces, 1998; Gerasimova et al., 2000, 2007; Pai et al., 2004; Golovnin et al., 2008, 2012; Ramos et al., 2011). Such results are not surprising, given that CP190 is a common component of both *gypsy* and dCTCF insulators and has been shown to colocalize to these structures previously (Pai et al., 2004; Gerasimova et al., 2007). However, BEAF-32 forms donut-shaped halos around the spherical bodies in stressed nuclei (Fig. 3 C) rather than colocalizing with the rest of the insulator proteins, a surprising finding given the substantial overlap between BEAF-32, CP190, and dCTCF at multiple genomic sites (Bushey et al., 2009). This arrangement of insulator proteins is maintained despite the overall size of the bodies, with the diameter of the spherical portion ranging from ∼200 nm to nearly 1 µm and the diameter of the surrounding BEAF-32 donuts being roughly proportionally double in size, meaning that these structures can approach sizes of >2 µm in extreme cases. Identical structures are also observed in S2 cells overexpressing BEAF-32::mCherry and Su(Hw)::EGFP, ruling out potential antibody artifacts (Fig. S2 A). Such findings suggest that although insulator bodies can vary widely in number and size, even within the same cell, they are highly ordered structures.

The position of these structures within the diploid nucleus is also peculiar. Most of the bodies appear to be in defined territories in the nuclear periphery (near the edges of the condensed chromatin mass) and in DAPI-less lacunas within the mass, suggesting these structures form in regions devoid of chromatin (Figs. 1 F and 4 A) and might be anchored to other nuclear structures, such as the nuclear lamina or the nuclear pore complex. Intensity correlation analysis revealed potential overlap between CP190 and lamin for a subset of insulator bodies in diploid cells; however, not all bodies are lamin associated, and small, punctate CP190 signals in unstressed cells also overlap with lamin (Fig. 4 A). Additionally, no significant colocalization between insulator bodies and nuclear pore components were observed (Fig. 4 B), suggesting that associations with lamin or nuclear pore complex components are not a requisite for insulator body formation. Furthermore, stressed S2 cells extracted with 2 M NaCl to isolate insoluble nuclear components (Byrd and Corces, 2003) revealed a loss of lamin-associated nuclear bodies, particularly in nuclei displaying a high extraction efficiency (>95% of soluble protein removed, large DAPI halo; Fig. 4 C). These data confirm that insulator bodies located in the nuclear periphery remain soluble and associate only transiently with the nuclear lamina.

Osmostress-induced insulator body formation can account for previously published studies of these structures

A comparison of our data with descriptions of these structures given in previous work, such as number, size, and nuclear distribution strongly suggests that the initially described insulator bodies are identical to the osmostress-induced insulator bodies described here (Gerasimova and Corces, 1998; Gerasimova et al., 2000, 2007; Ghosh et al., 2001; Pai et al., 2004; Xu et al., 2004; Capelson and Corces, 2005, 2006; Lei and Corces, 2006; Golovnin et al., 2008, 2012; Ramos et al., 2011; Wood et al., 2011). If this is true, an obvious question arises: how might these structures have arisen in previous studies? We found that both the choice of buffer and time of dissection until fixation dictated whether tissue displayed insulator body

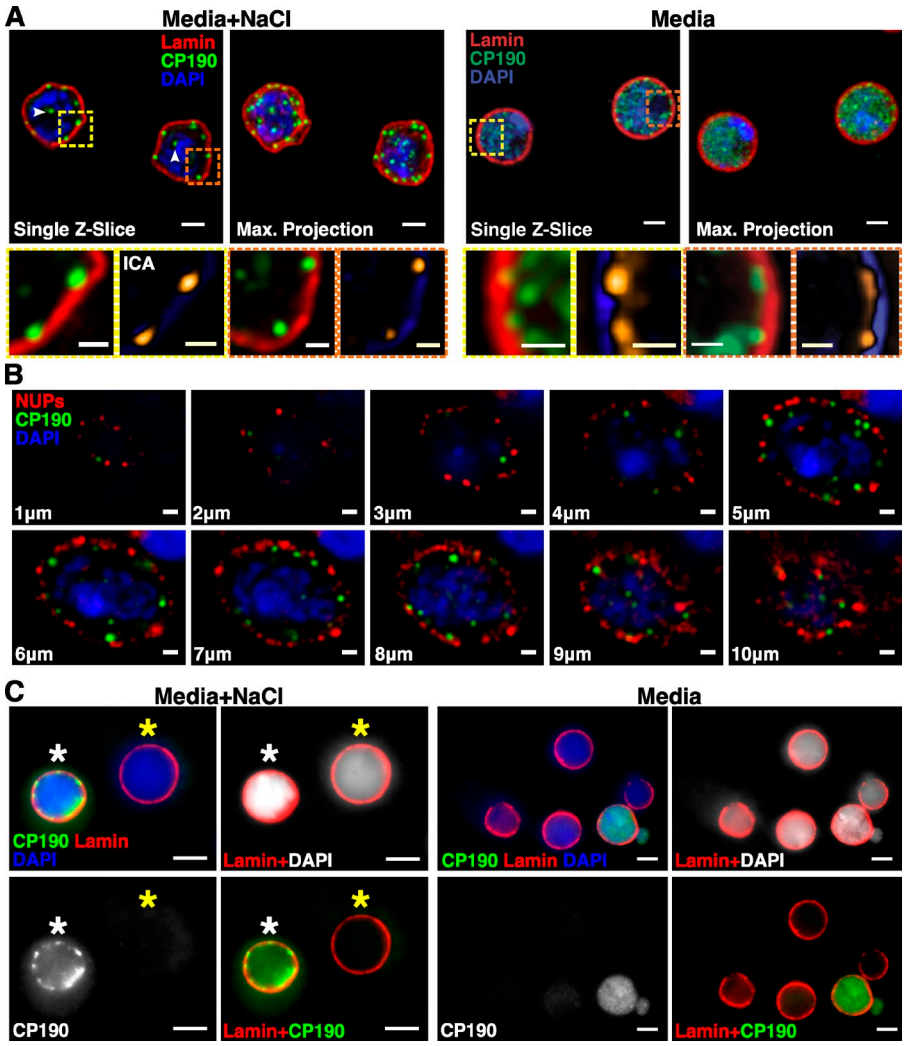

Figure 4. **Insulator bodies localize to DAPI-less regions and associate transiently with the nuclear lamina.** S2 cells treated with or without 250 mM NaCl and stained for CP190 and lamin. (A) Bodies localized to the interior form in DAPI-less lacunas (white arrowheads). Intensity correlation analysis (boxed regions and insets) reveals regions of high overlap (gold) between CP190 bodies in the nuclear periphery and lamin. (B) Serial 1-µm z slices through a S2 nucleus stressed with 250 mM NaCl stained for CP190 and nuclear pore complex components (NUPs). (C) Nuclear halos generated from 250 mM NaCl-stressed S2 cells showing a highly extracted nucleus with no CP190 signal (yellow asterisks) and a less efficiently extracted nucleus (white asterisks) showing remnants of CP190 bodies colocalized with lamin. Bars: (A, main images) 2 µm; (A, insets) 0.5 µm; (B) 1 µm; (C) 4 µm.

formation or not (see Materials and methods). Larval tissue dissected rapidly in 100 µl SFX media or PBS (<5 min) retained the diffusely speckled pattern, whereas dissection in *Drosophila* Ringer's solution led to the rearrangement of CP190 and Mod to the nuclear periphery and formation of insulator bodies. (Fig. 5 A). Interestingly, incubating tissues in either SFX or PBS for >30 min under nonhumidifying conditions lead to the formation of insulator bodies (Fig. 5 B). SFX media–treated tissues formed a single large body, contiguous with diffusely speckled protein located primarily in the nuclear periphery. PBS incubation led to the formation of smaller, but more numerous, bodies in the periphery contiguous with a smaller proportion of diffusely speckled protein, a morphology identical to the aforementioned previously published studies and to tissue treated with 250 mM NaCl (Fig. 1 D). Similar results were obtained in S2 cells incubated with PBS or Ringer's solution, with cells near the edge of the liquid showing a more robust response (Fig. 5 C). This observation, coupled with the considerable H_2O evaporation and subsequent increase in solute concentration noted after >30-min tissue incubations under nonhumidifying conditions irrespective of buffer, likely explains how these structures were previously generated in the absence of purposeful induction.

Insulator bodies form rapidly after stress, display highly dynamic behavior during the duration of stress, and are readily reversible

The drastic change in the nuclear distribution of insulator proteins in osmotically stressed versus unstressed nuclei suggested a highly dynamic transition between the two states. Using fluorescently tagged versions of BEAF-32 and Su(Hw), we were able to track the progression of insulator body formation in S2 cells during osmostress. Both BEAF-32 and Su(Hw) appear to nucleate from smaller speckles, creating larger structures—this correlates with the gradual disappearance of diffusely speckled signal throughout the nucleus as the bodies become larger and their fluorescent intensity increases, over an order of minutes as the salt concentration gradually increases to 250 mM (Fig. 6 A and Video 1). As the duration of time exposed to salt increases, the bodies remain roughly the same size and exhibit highly variable dynamics. Some bodies remain localized close to their sites of nucleation, with minimal movement, whereas others move readily and undergo rounds of fusion to create larger bodies, whose movement throughout the nuclear periphery appears constrained by the nuclear lamina and the chromatin mass (Fig. 6, B and C).

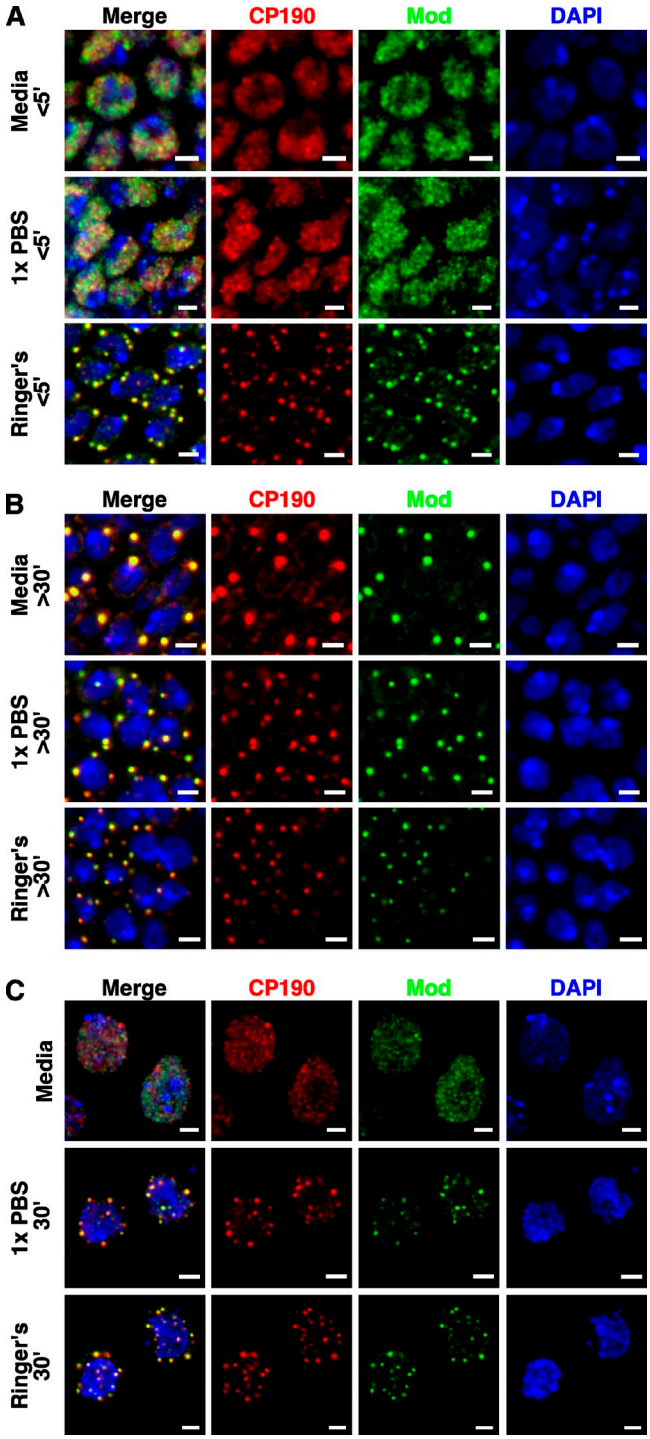

Figure 5. **Buffer choice and tissue dissection conditions can account for insulator body formation.** (A and B) Wing discs from third instar larvae dissected in SFX media, PBS, or *Drosophila* Ringer's solution and fixed in <5 min (A) or after a 30-min incubation in nonhumidified conditions (B), stained for CP190 and Mod(mdg4). (C) S2 cells show a similar response after a 30-min incubation in PBS or Ringer's solution (media controls were kept humidified to prevent evaporation). Bars, 2 µm.

FRAP analysis of stationary Su(Hw)::EGFP bodies suggests that these structures undergo rapid protein turnover, with recovery half-times on the order of seconds (4–15 s) despite a relatively small fraction of free protein (mobile fraction 30–45%; Fig. S2 B).

In addition to their rapid formation, insulator bodies disappear equally as quickly once cells are returned to isotonic media. Using the same C-terminally tagged Su(Hw)::EGFP used in S2 cells, we generated transgenic flies containing this construct under *UAS*/Gal4 control. Polytene chromosome squashes and chromatin immunoprecipitation (ChIP) with α-GFP verified its DNA-binding ability, whereas expression in the wing margin of cut^{6}; $su(Hw)^{e04061}$ restores *gypsy* insulator function, confirming that the tagged construct accurately reproduces the enhancer-blocking behavior of endogenous Su(Hw) (Fig. S2, C–E). Using explanted salivary glands dissected from third instar larvae expressing this construct, we tested whether insulator body formation is reversible once osmostress is alleviated. Before salt addition, DNA-bound Su(Hw)::EGFP is distributed exclusively along polytene chromosomes from salivary glands (Fig. 6 D). Within ∼60 s of salt addition, this pattern is disrupted, and throughout the duration of stress, Su(Hw) continues to relocate into bodies, with some individual foci drawing together to produce larger fusions. Remarkably, by the time the first recovery frame is acquired (∼2 min), these bodies have disappeared and the Su(Hw) signal is once again distributed on the chromosomes, which persists as the chromosomes continue to expand to their prestressed state. Interestingly, bands of Su(Hw) visible before stress are restored with a nearly identical spatial distribution in the nucleus after recovery (Fig. 6 D and Video 2). Furthermore, diploid tissue subjected to two rounds of salt treatment and recovery show similar behavior, with body formation and disassembly kinetics nearly identical between both rounds of treatment (Videos 3 and 4).

Insulator body formation correlates with a reduction of chromatin-bound insulator proteins

Given the distinct localization of these structures to DAPI-less regions of the stressed diploid nucleus, we hypothesized that insulator bodies may not the attached to chromatin as previously thought. We first compared the distribution of CP190 on polytene chromosomes from osmostressed and control salivary glands from third instar larvae. Whole-mount staining of intact nuclei from media controls revealed multiple bands of CP190 that overlapped extensively with the chromosome arms (Fig. 7 A), reflecting the chromatin-bound state of this protein. However, these bands were absent from osmostressed nuclei, and virtually all of the CP190 was instead confined to insulator bodies located in the nuclear periphery and interior spaces between the chromosome arms (Fig. 7 B), strongly suggesting that insulator proteins are removed from chromatin to form bodies.

To verify, we used ChIP to biochemically measure chromatin removal during osmostress. Using S2 cells, we tested chromatin enrichment during stress at three types of Su(Hw) insulators: the *gypsy* insulator (Su(Hw), CP190, and Mod(mdg4)67.2), the *homie* super insulator (all known insulator proteins; Fujioka et al., 2009), and an endogenous intragenic insulator (3L:12247800) that binds only to Su(Hw). All stressed samples show an ∼50–80% decrease in the amount of chromatin-bound Su(Hw) compared with media-only controls, depending on the insulator. Both *gypsy* and the Su(Hw)-only insulator show the largest decrease

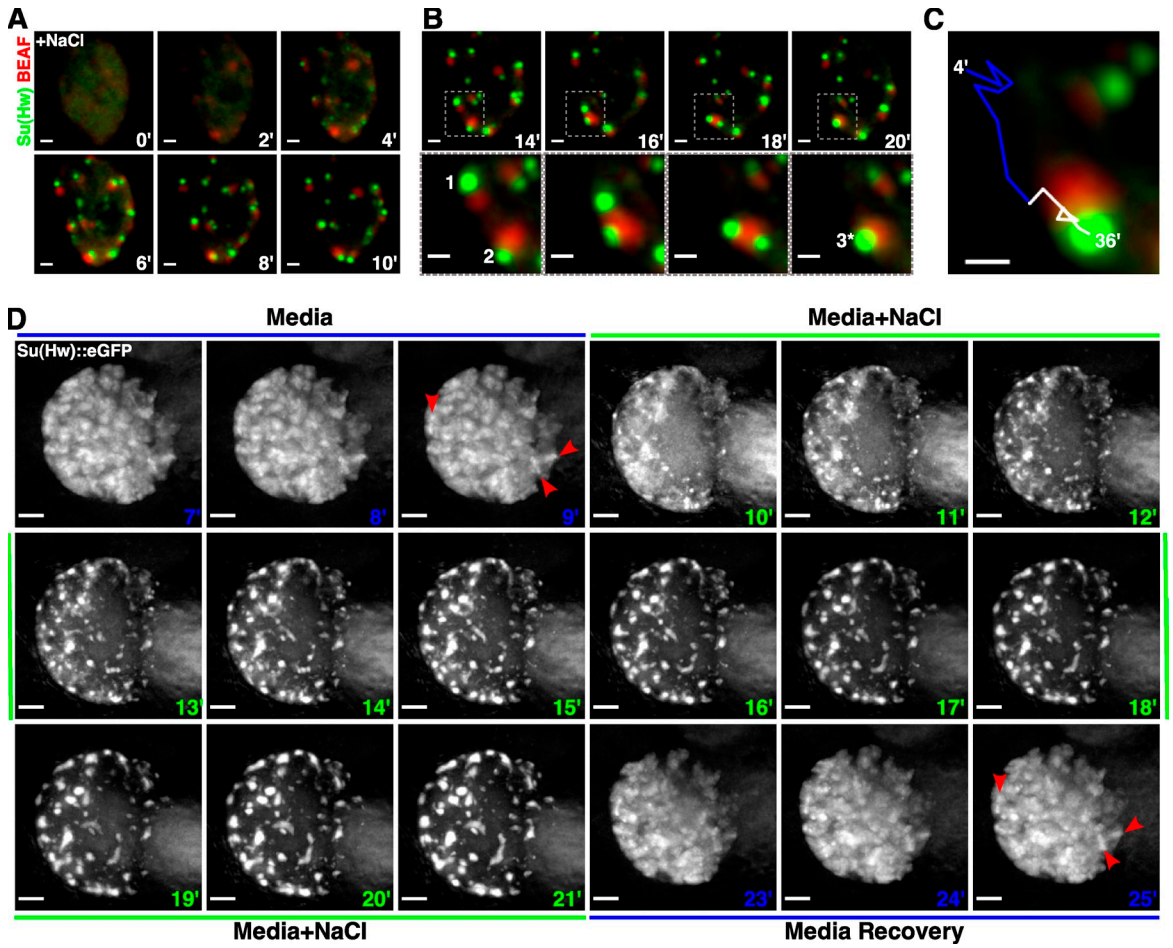

Figure 6. **Insulator body formation and disassembly occurs rapidly, and bodies are highly dynamic.** (A and B) Frames taken at 2-min intervals after gradual 250 mM NaCl media addition at time 0 min in S2 cells expressing Su(Hw)::EGFP and BEAF-32::mCherry. Bodies form in a matter of minutes from diffuse speckles (A) and can undergo rounds of fusion (bodies 1 and 2) to produce larger structures (body 3*; B). Boxed regions are enlarged in insets at the bottom. (C) The dynamic movement of body 1 starting with its formation at 4 min until its fusion with body 2 at 20 min (blue line) and the movement of the fused body (white line) until the final frame was acquired (36 min). (D) A polytene nucleus from a third instar salivary gland expressing Su(Hw)::EGFP subjected to 250 mM NaCl osmostress (10 min) followed by recovery in isotonic media (23 min). Blue numbers denote media treatment time points, and green numbers indicate stress treatment time points. Arrowheads (9 and 25 min) mark bands of Su(Hw). Bars: (A, B [top], and D) 3 µm; (B [bottom] and C) 2 µm. Also see Videos 1, 2, 3, and 4.

(~80%), whereas *homie* shows less of a reduction (~50%; Fig. 7, C–E). We have also observed similar reductions in Su(Hw) enrichment at these insulators in cells treated with sucrose, in addition to seven other Su(Hw) binding sites, suggesting that this behavior is not restricted to a specific subset of insulators or is caused by the biophysical effects of NaCl. Additionally, 3C (chromosome conformation capture) experiments further support the idea of chromatin removal during stress, as looping contacts at the *muscleblind* locus that are disrupted in Su(Hw) knockdown cells are similarly disrupted after osmostress (Fig. S2 F and not depicted).

This data, combined with our Su(Hw)::EGFP live-imaging stress and recovery results, suggested a model in which insulator body formation correlates with a reduction in chromatin-bound insulator proteins that is restored upon recovery as the bodies disassemble and the normal chromatin architecture is restored. To test this hypothesis, we measured Su(Hw) enrichment at each insulator after 2.5-min recovery in isotonic media after 20-min osmostress. Not surprisingly, Su(Hw) enrichment after recovery is restored to levels greater than or equal to those observed for media controls (Fig. 7, C–E), verifying that insulator body formation can be used as a proxy to monitor the chromatin-bound state of insulator proteins.

Differential requirement for insulator protein recruitment to insulator bodies

Given that insulator bodies are highly ordered structures containing a reproducible arrangement of insulator proteins (Fig. 3), we wondered whether removal of any one protein would disrupt their formation. Previous work has suggested that full-length CP190 is required for formation of insulator bodies marked with Su(Hw) and Mod(mdg4)67.2 in both S2 cells and larval tissue (Pai et al., 2004; Golovnin et al., 2012). However, shRNA-mediated knockdown of CP190 in the posterior compartment of wing discs from third instar larvae using a *UAS-Dcr-2; engrailed-Gal4* driver did not disrupt the ability of Mod(mdg4)67.2 to form bodies under conditions of osmostress, which were morphologically identical to those formed in the anterior compartment

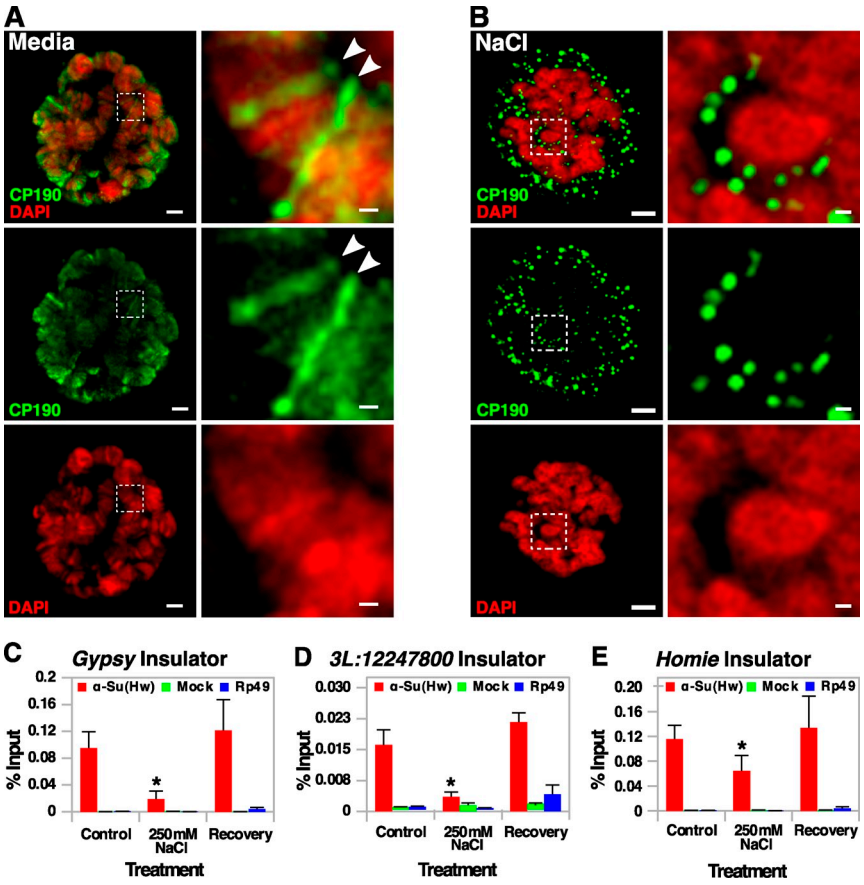

Figure 7. **Insulator body formation correlates with a reduction in chromatin-bound Su(Hw) that is rapidly restored upon return to isotonicity.** (A) A media-treated salivary gland polytene nucleus labeled with CP190 showing the expected band pattern (insets, arrowheads). (B) A polytene nucleus stressed with 250 mM NaCl labeled with CP190 shows bodies in the nuclear periphery and interchromosomal spaces lacking DAPI (insets). (A and B) Boxed regions are enlarged in insets on the right. (C–E) ChIP of Su(Hw) at *gypsy* (C), 3L:12247800 (D), and *homie* insulators (E) in media, stressed, and recovery S2 cells. Asterisks mark reductions significantly different from media controls (Student's paired *t* test, P = 0.05; error bars represent SEMs). Bars: (A and B, main images) 3 µm; (A and B, insets) 0.5 µm.

containing wild-type levels of CP190 (Fig. 8 A). Conversely, double-stranded RNA (DsRNA)–mediated knockdown of CP190 in S2 cells did impair the ability of Mod(mdg4)67.2 to form bodies during osmostress, remaining diffusely speckled despite extensive chromatin condensation. Interestingly, even small amounts of CP190 present after incomplete knockdown leads to nucleation of small bodies marked by both CP190 and Mod(mdg4)67.2 in these cells (Fig. S3 A).

To confirm that CP190 does not significantly influence Mod(mdg4)67.2 insulator body behavior in tissue, we took advantage of two trans-heterozygous CP190 allele combinations ($CP190^{H31\text{-}2}/CP190^{P11}$ and $CP190^{4\text{-}1}/CP190^{P11}$) given that flies carrying CP190 homozygous null mutations are embryonic lethal (Pai et al., 2004). $CP190^{P11}$ is a large deletion removing the entire CP190 locus, $CP190^{H31\text{-}2}$ produces a truncated CP190 protein possessing only the N-terminal BTB (Broad Complex, Tramtrack, and Bric-a-brac) domain as a result of a point mutation that truncates a splice junction, and the $CP190^{4\text{-}1}$ allele produces a larger truncation missing only part of the C-terminal Glu-rich domain as a result of a nonsense mutation (Fig. 8 B). In either CP190 allele combination, Mod(mdg4)67.2 body formation was readily observable not only in wing discs but also in other larval tissue (brains, other imaginal discs, and salivary glands; Fig. 8 B and not depicted) and indistinguishable from balanced controls. Such findings are in agreement with shRNA depletion of CP190 (Fig. 8 A) and suggest that Mod(mdg4)67.2 can form bodies independently of CP190 in larval tissue.

Interestingly, null mutations in *mod(mdg4)67.2* (*mod(mdg4)^{u1}*) disrupted the ability of Su(Hw), but not CP190, to enter insulator bodies in wing discs during osmostress (Fig. 8 C). In the absence of Mod(mdg4)67.2, Su(Hw) remained diffusely distributed exclusively in the nuclear periphery, surrounding the condensed chromatin mass, whereas CP190 formed insulator bodies. Only when Mod(mdg4)67.2 was present did Su(Hw) enter CP190-marked bodies, suggesting that interactions between Mod(mdg4)67.2 and Su(Hw), but not CP190 and Su(Hw), are required for Su(Hw) to enter insulator bodies. Finally, mutations in *su(Hw)* did not alter the ability of CP190 or Mod(mdg4)67.2 to form insulator bodies in larval tissue (Fig. S3 B), whereas BEAF-32 recruitment to CP190- and Mod(mdg4)67.2-marked bodies was not impaired by reductions in any of the three *gypsy* components (unpublished data). Taken collectively, these data suggest that protein recruitment to insulator bodies relies on a complex network of protein–protein interactions that may be cell/tissue specific.

Insulator body formation is independent of the dMEKK1-p38 osmostress-sensing pathway

Next, we attempted to elucidate the mechanism responsible for controlling insulator body formation. We focused on the highly conserved HOG–MAPK pathway, given its central role in mediating the osmostress response in virtually all eukaryotes (Saito and Posas, 2012). Activation leads to cell cycle arrest, increased synthesis of intracellular osmolytes, and fine tuning of transcription

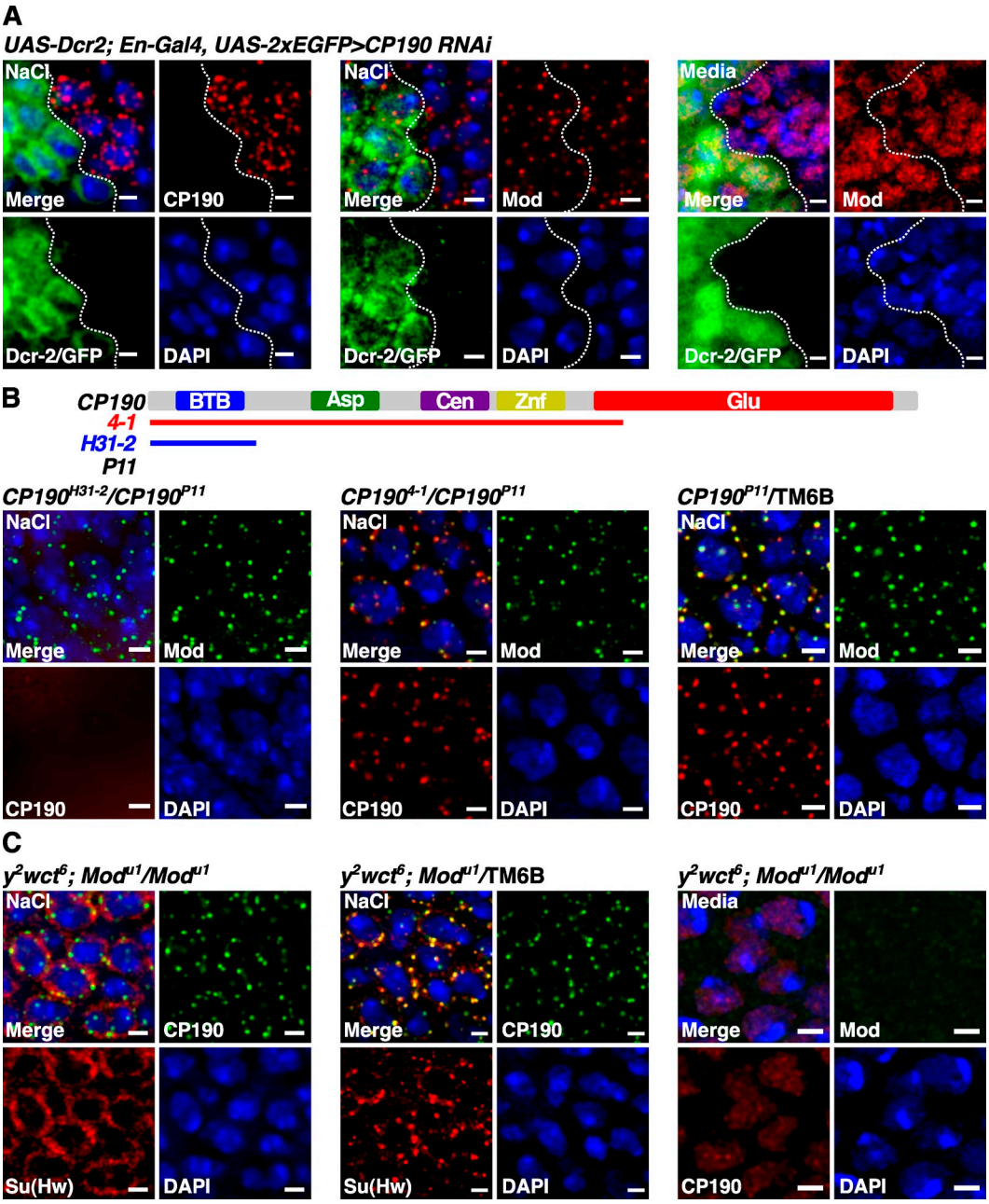

Figure 8. **CP190 and Mod(mdg4) enter bodies independently of one another, but Su(Hw) requires Mod(mdge4) in larval tissue.** (A) Wing discs from CP190-RNAi larvae stressed with 250 mM NaCl and labeled with CP190 (left) or Mod(mdg4) (middle). Unstressed controls labeled with Mod(mdg4) are shown on the right. GFP marks Dcr-2$^+$ knockdown cells, and the dashed lines demarcate the anterior–posterior axis of the wing disc. (B) Wing discs from two trans-heterozygous CP190 mutant larvae, $CP190^{H31\text{-}2}/CP190^{P11}$ (left) and $CP190^{4\text{-}1}/CP190^{P11}$ (middle) and a balanced control containing full-length CP190 (right) stressed with 250 mM NaCl and stained with CP190 and Mod(mdg4). Note that our CP190 antibody recognizes the $CP190^{4\text{-}1}$ isoform but not the $CP190^{H31\text{-}2}$ isoform. Domains of CP190 (BTB, Asp rich [Asp], microtubule binding [Cen], Zinc finger [Znf], and Glu rich [Glu]) present in each truncated allele are indicated by the colored lines. (C) Wing discs from null mod^{u1} homozygotes (left) and balanced heterozygotes (middle) stressed with 250 mM NaCl and stained with Su(Hw) and CP190. (right) Mod staining verifies absence of protein in the mod^{u1} mutant. Bars, 2 µm.

and translation to allow cells to tolerate hyperosmotic conditions that would otherwise trigger cell death. At the core of this pathway is a MAPK cascade that in flies includes the upstream MAPKKK, *dMekk1*, and the downstream effector MAPK *p38*. *Drosophila* contains two *p38* genes, *p38a* and *p38b*, which mediate the response to a variety of environmental stressors in a partially redundant manner. *p38b* and *dMekk1* are required for osmostress tolerance, whereas *p38a* appears to be dispensable (Han et al., 1998; Inoue et al., 2001; Craig et al., 2004). However, mutations in either *dMekk1* ($dMekk1^{UR36}$; Inoue et al., 2001) or p38a and p38b ($p38a^{del}$, $p38b^{\Delta 25}$, and $p38b^{\Delta 45}$; Vrailas-Mortimer et al., 2011) failed to suppress CP190 insulator body formation (Figs. 9, A–D; and S4, A–C), as did RNAi-mediated knockdown of *JNK* (*basket*), another MAPK that is activated by Mekk1 under conditions of hyperosmolarity in mammalian cells (Figs. 9 E and S4 D; Yujiri et al., 1999). Taken

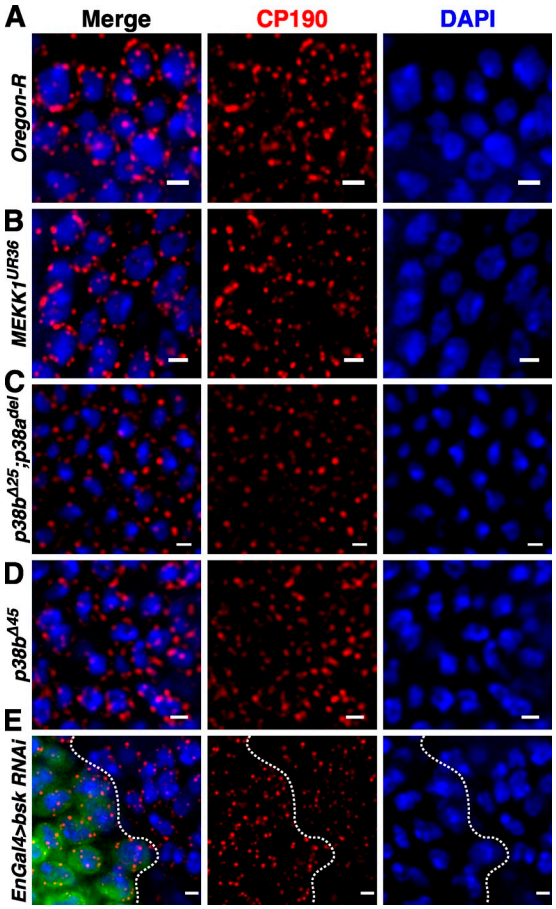

Figure 9. **Insulator body formation is independent of the HOG–MAPK osmostress pathway.** (A–E) Wing discs from Oregon-R (A), *dMEKK1*^{UR36}/*dMEKK*^{UR36} (B), *p38b*$^{\Delta 25}$;*p38a*^{del}/*p38b*$^{\Delta 25}$;*p38a*^{del} (C), *p38b*$^{\Delta 45}$/*p38b*$^{\Delta 45}$ (D), and *bsk (JNK)-RNAi* (GFP marks Dcr-2^{+} knockdown cells, and the dashed lines demarcate the anterior–posterior axis of the wing disc; E) stressed with 250 mM NaCl and stained with CP190. Bars, 2 µm.

collectively, these findings suggest that insulator body formation is independent of the canonical HOG–MAPK osmostress sensing pathway.

Insulator bodies are also evident in apoptotic nuclei

Given that insulator proteins form bodies readily in response to osmostress independently of the HOG–MAPK pathway, we wondered whether other cellular pathways might also trigger formation. We focused on cell death, particularly apoptosis, given the morphological similarities between cells in the initial stages of apoptosis and those under osmotic shock (Burg et al., 2007). To test this hypothesis, we examined eye/antennal discs from Drop^{Mio} third instar larvae, in which retinal precursor cells undergo cell death caused by arrested furrow progression (Mozer, 2001). In death regions, CP190 forms bodies in a subset of apoptotic nuclei (marked with cleaved caspase-3) reminiscent of those induced during osmostress, whereas those cells not marked as apoptotic contain diffusely speckled CP190 signal distributed throughout the nucleus (Fig. S5, A and B). Similar results were obtained with Bar^{S} eye discs as well, with BEAF-32 foci readily observable in these apoptotic tissues as well (unpublished data). Thus, both osmostress and cell death trigger formation of insulator bodies.

Discussion

Our results demonstrate that insulator bodies are a novel class of nuclear stress bodies, which to our knowledge has yet to be described in any eukaryote in response to osmostress. Our data suggest a model in which insulator proteins are removed from chromatin and form bodies in distinct nuclear territories, which are maintained throughout the duration of osmostress by constant turnover of proteins. Once the stress response is alleviated, the bodies rapidly disassemble as the individual proteins migrate back to their cognate binding sites, restoring the normal chromatin architecture observed before stress (Fig. 10). Other nuclear stress bodies have been described in both *Drosophila* and mammals in response to heat shock, consisting of heterogeneous nuclear RNPs and transcription factors required for rapid induction and processing of heat shock–responsive genes that allow the cell to adapt to elevated temperatures (Biamonti and Vourc'h, 2010). Whether insulator bodies play a functional role in the cellular response to osmostress remains to be elucidated; however, given the potential epigenetic consequences of both heat shock and osmostress (Seong et al., 2011), it is likely that a better understanding of the relationship between stress and nuclear dynamics will reveal additional mechanisms underlying environmentally induced changes in genome function.

Our findings in light of previous work raise the question of whether osmostress-induced insulator bodies are the "same" as those identified in past studies (Gerasimova and Corces, 1998; Gerasimova et al., 2000, 2007; Ghosh et al., 2001; Pai et al., 2004; Xu et al., 2004; Capelson and Corces, 2005, 2006; Lei and Corces, 2006; Golovnin et al., 2008, 2012; Ramos et al., 2011; Wood et al., 2011). Previous characterization of these structures has relied on three main criteria: the number of bodies per diploid nucleus (10–30), their nuclear distribution (nuclear periphery), and extensive colocalization between insulator proteins. Our data satisfy all of these requirements, and we argue that osmostress-induced insulator bodies are identical to those published previously—if not for the simple reason that we were unable to observe these structures in any other cellular context. Furthermore, we have provided a likely explanation of how these structures may have arisen in the absence of purposeful induction. Insulator body formation does not occur in small volumes of PBS if tissues are dissected and fixed rapidly (<5 min); however, extended tissue dissections before fixation in small volumes of PBS under nonhumidifying conditions (i.e., on the benchtop/under the stereoscope) lead to the formation of insulator bodies that are identical to those purposefully treated with elevated NaCl, sorbitol, or sucrose, making it simple to envisage how these structures formed in previous studies. Perhaps most importantly, however, is that this also creates the potential for misinterpretation of data. Our NaCl gradient results suggest that the robustness of the insulator body response correlates with the severity of the osmostress, which could lead to a range of insulator body phenotypes if the initial

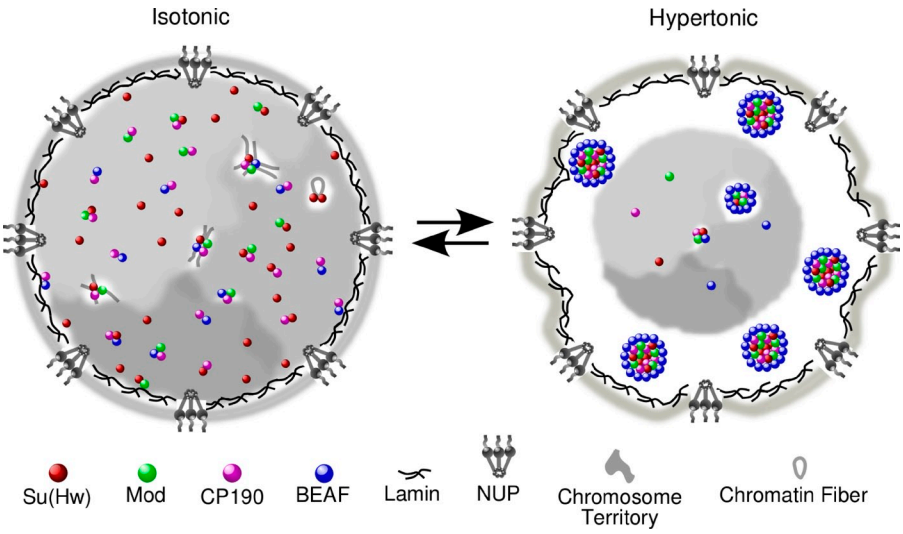

Figure 10. **A model for insulator body formation during osmostress and cell death.** NUP, nuclear pore complex.

dissection and incubation conditions before fixation are not properly controlled between samples being compared. We therefore urge caution in using these structures as a metric of insulator function/activity, unless such controls are implemented.

Along these lines, we have provided direct biochemical evidence that these structures are not the physical manifestations of multiple DNA-bound insulator proteins, as chromatin-bound Su(Hw) is dramatically reduced during body formation. Given that insulator properties, such as enhancer/heterochromatin blocking and chromatin looping are conferred by insulator proteins physically bound to DNA, it is extremely unlikely that these structures contribute to these processes during osmostress. Although we cannot rule out that there may be a handful of insulator sites that do not lose their proteins and instead act to nucleate and tether these structures to chromatin, we argue that this is unlikely for the following reasons: first, immunostaining in stressed polytene chromosomes reveals complete loss of the characteristic CP190 bandlike signals rather than an increase in signal at a handful of binding sites, which would be expected if they acted as nucleation hubs. Additionally, unlike diploid cells in which DAPI would likely lack the sensitivity to detect the presence of a few peripherally associated chromatin fibers that might still remain attached to bodies after global chromatin condensation, the organization of polytene chromosomes ensures that individual chromatids remain in close association with one another, and there is a clear demarcation between peripherally localized bodies and chromatin when polytene chromosomes condense. Nonetheless, ChIP sequencing coupled with immuno-FISH of potential nucleation sites will be needed to accurately address this possibility.

It is interesting to point out that the distribution of insulator proteins in unstressed diploid cells, consisting of hundreds of tiny speckles distributed throughout the volume of the nucleus, are morphologically similar to PcG bodies that have been shown to be functionally relevant given that they physically colocalize with DNA to contribute to Hox gene silencing (Bantignies et al., 2011). We favor the idea that insulator speckles under unstressed conditions also reflect the functional state of DNA-bound insulator proteins and are likely the physical manifestations of localized chromatin looping between insulator sites to establish chromatin domains. This is supported by the fact that there are distinct speckles for each insulator protein that overlap with other insulator proteins at some, but not all speckles, likely to be a reflection of the combinatorial binding of insulator proteins to different sites as measured by ChIP (Bushey et al., 2009; Nègre et al., 2010). Now that high-resolution looping maps of the *Drosophila* genome are available (Hou et al., 2012; Sexton et al., 2012), it would be possible to test this using immuno-FISH, particularly between physical domain borders that have been shown to undergo long-range looping contacts and are demarcated by specific combinations of insulator proteins (Hou et al., 2012).

As for the structures themselves, it is important to reiterate that they do not appear to be insoluble aggregates of randomly associated proteins. Insulator bodies do not colocalize with mCherry-tagged version of Hsp70, Hsp40, or Pros54 (a 26S proteasome subunit), suggesting that these structures are not sites of unfolded proteins or those targeted for degradation (unpublished data). They contain a reproducible arrangement of insulator proteins within these structures, exemplified by the presence of BEAF-32 as a donut-shaped pattern around a spherical core of CP190, dCTCF, Su(Hw), and Mod(mdg4)67.2. Other donut-shaped nuclear bodies have been described using electron microscopy, such as promyelocytic leukemia bodies and clastosomes (Zhong et al., 2000; Lafarga et al., 2002), and it is possible that even the spherical proteins also manifest themselves as ring or donut structures that are not readily observable given the resolution limits of light microscopy. Future super resolution imaging and electron microscopy will be critical for understanding the organization of these structures. Furthermore, biochemical isolation of these structures followed by mass spectrometry will be required to identify the large number of proteins involved, which will be crucial for identifying novel insulator proteins and other interacting partners, potential posttranslational modifications required for body formation, and perhaps providing insight into what the functional role of these structures might be.

Given this relatively ordered structural arrangement dictated by protein–protein contacts, it might be expected that a loss of certain core "scaffolding" proteins would suppress insulator body formation. Though this is difficult to assess globally because we still do not know the full complement of proteins that are in these structures, it was recently shown in S2 cells that DsRNA-mediated knockdown of CP190 disrupts the ability of Mod(mdg4) to enter bodies, whereas similar reductions in Mod(mdg4) impairs the ability of Su(Hw), but not CP190, to enter bodies (Golovnin et al., 2012). Interestingly, we found a similar CP190 dependence for Mod(mdg4) in S2 cells, but not larval tissue, in which Mod(mdg4) was still able to enter bodies independently of CP190. This was confirmed not only in CP190 shRNA–depleted tissue but also in two other CP190 truncated mutants as well that had previously been shown to disrupt Mod(mdg4) localization in tissue (Lei and Corces, 2006), though this was likely caused by misinterpretation as outlined (see Discussion, second paragraph). However, Mod(mdg4) was required for Su(Hw) to localize to CP190 bodies in tissues, in agreement with previous work in S2 cells (Golovnin et al., 2012). One interpretation of our results would be that there are tissue/cell type–specific requirements for proteins to be recruited to insulator bodies, such as the availability of other proteins, posttranslational modifications, or even RNA. For example, Mod(mdg4) could be recruited to bodies in a redundant manner, by either CP190 or some tissue-specific protein/RNA that is present in larval tissue but not S2 cells. A more likely possibility, however, involves differences in posttranslational modifications to the proteins themselves. We find that CP190 is SUMOylated in response to osmostress in S2 cells that is removed upon recovery (Fig. S4, E–G); however, SUMOylated Mod(mdg4) or Su(Hw) was not detected under the same conditions with our antibodies, which might be the result of epitope masking. Interestingly, CP190, Mod(mdg4), and Su(Hw) all contain computationally predicted small ubiquitin-like modifier (SUMO) interacting motifs, which for Mod(mdg4) happens to be within the Q-rich domain, which has been shown to be necessary for its localization to bodies in S2 cells and also contains a SUMOylation motif required for body formation (Golovnin et al., 2008, 2012). Perhaps this SUMO interacting motif mediates Mod(mdg4)'s interaction with SUMOylated CP190 in S2 cells, which would explain its dependence on CP190 in this cell type. Nonetheless, it will be important for future work addressing the role of SUMO in body formation to take into account potential discrepancies between cell/tissue types.

Additionally, we have yet to identify a signal transduction pathway that might coordinate these potential posttranslational modifications. We have ruled out the canonical HOG–p38 MAPK osmostress sensing pathway; however, it is interesting that these structures are also present in a subset of apoptotic nuclei. The phenotypic similarities between the two processes, such as cell volume reduction, chromatin condensation, and disrupted lamin suggests that the two might not be mutually exclusive and may share similar signaling pathways (Burg et al., 2007), which might involve both biological and mechanical/biophysical cues. Future characterization of the link with apoptosis may be critical to resolving these issues, in addition to future studies addressing the role of molecular crowding in this phenomenon (Richter et al., 2008).

Finally, the physiological significance of chromatin removal and insulator body formation remains unknown. It appears not to be required for chromatin compaction or to directly induce changes in gene expression (Fig. S5, C–E; and not depicted). Heat shock has been shown to reduce chromatin-bound CP190, but presumably not other insulator proteins, and does not lead to body formation (Oliver et al., 2010; Wood et al., 2011), suggesting that this phenomenon may be restricted to osmostress. It is intriguing that other types of chromatin binding proteins do not show a dramatic reorganization during osmostress, and given the central role insulators play in organizing the chromatin fiber into higher order structures, we favor the idea that insulators do play a functional role in the osmostress response and are specifically targeted to form bodies. Perhaps removal of insulators from DNA is needed to disrupt or reorganize chromatin domains that are needed for the genome to execute otherwise quiescent gene regulatory programs to adapt to osmostress. In such a state, the nucleus would be primed for rapid recovery once the stress is alleviated, as the insulator proteins stored in the bodies would be readily available to rebind chromatin, reestablishing the domains present in the unstressed state and restoring the default chromatin architecture for that cell type. Future high throughput studies, including RNA/ChIP sequencing and genome-wide 3C to examine global changes in transcript levels, chromatin-bound insulator proteins, and looping contacts, will be necessary for testing such a hypothesis.

Materials and methods

Fly stocks and husbandry

All stocks and crosses were maintained on standard cornmeal-agar media at 25°C. Microinjection to generate transgenic lines *yw; P{SuHw::EGFP, w+}* was performed by GenetiVision. Bloomington Stock Center lines are as follows: $y^1sc^*v^1$; *P{TRiP.HMS00845}attP2* (CP190 RNAi, stock #33903); y^1v^1; *P{TRiP.JF01275}attP2* (JNK RNAi, stock #31323); *P{UAS-Dcr-2.D}*^{1}, w^{1118}; *P{en2.4-GAL4}*^{e16E}, *P{UAS-2×EGFP}AH2* (stock #25752); *w*; P{GAL4-vg.M}2; TM2/TM6B, Tb*^{1} (stock #6819); and w^{1118}; *PBac{RB} Su(Hw)e04061/TM6B, Tb*^{1} (stock #18224). CP190 mutants (V. Corces, Emory University, Atlanta, GA) are as follows: y^2wct^6; *CP190*$^{H31\text{-}2}$/TM6B, *Tb*^{1}, y^2wct^6; *CP190*$^{4\text{-}1}$/TM6B, *Tb*^{1} and *CP190*^{P11}/TM6B *Tb*^{1}. Gal4 drivers are as follows: *yw; Hsp70-Gal4/*Cyo (B. McKee, University of Tennessee, Knoxville, TN) and *w*; GMR-Gal4* (T. Dockendorff, University of Tennessee, Knoxville, TN). *Mekk1* mutant (H.D. Ryoo, New York University Langone Medical Center, New York, NY) was *FRT82B, MeKK1*^{UR36}/TM6B, *Tb*^{1}. *p38* mutants (A. Vrailas-Mortimer, Emory University School of Medicine, Atlanta, GA) were *p38b*$^{\Delta 45}$ and *p38b*$^{\Delta 25}$/Cyo, *GFP; p38a*^{del}. Our laboratory generated lines y^2wct^6; *mod(mdg4)*^{u1}/TM6B, *Tb*^{1}; *yw; Dr*^{Mio}/TM6B, *Tb*^{1}; y^2wct^6; *P{Su(Hw)::EGFP}*/Cyo; *Su(Hw)*^{e04061}/TM6B, *Tb*^{1}; and y^2wct^6; *P{GAL4-vg.M}2; Su(Hw)*^{e04061}/TM6B, *Tb*^{1}. RNAi crosses were maintained at 29°C to induce high levels of knockdown.

Expression vector construction

The pMK33-CTAP (C-terminal Tandem Affinity Purification) tag vector backbone (Veraksa et al., 2005) was used to generate dual-expression constructs containing both Su(Hw)-EGFP and mCherry coding sequences under the control of the copper-responsive metallothionein promoter. Su(Hw) (amplified from ovary cDNA) and EGFP were fused in frame and inserted into the XhoI–SpeI sites of pMK33-CTAP using the HD cloning system (In-Fusion; Takara Bio Inc.) creating a C-terminally tagged construct. From this vector, the metallothionein promoter was amplified with primers designed with a 3′ NheI site and stitched back into the pMK33 NotI site using the In-Fusion system. Next, the mCherry coding sequence was amplified from pAN583 (gift from A. Nebenführ, University of Tennessee, Knoxville, TN) with

primers containing 5′ AvrII–BswiI–AgeI sites and 3′ EcoRV–KpnI–MluI sites and fused into the 3′ NheI site downstream of the newly inserted metallothionein promoter. Final construction of the dual-expression vector was achieved by simply amplifying a coding sequence of interest (CP190, BEAF-32, CTCF, H2Av, etc.) and inserting it into either the 5′ or 3′ cut sites flanking mCherry to create C- or N-terminally tagged fusions. Fly expression constructs were generated using the pUAST-Y vector backbone containing a 5× UAS, minimal Hsp70 promoter, and w^+. SuHw::EGFP was amplified from pMK33 and inserted into XhoI–XbaI sites using the In-Fusion HD cloning system.

Antibodies

Rat and rabbit polyclonal IgG antibodies generated against full-length Su(Hw) and CP190 and Mod(mdg4)67.2 lacking only the BTB domains were previously generated in our laboratory (Wallace et al., 2010) and used at the following dilutions for immunostaining: Su(Hw), 1:50–1:300; CP190, 1:500–1:1,000; and Mod(mdg4)67.2, 1:250. Other antibodies used were α-lamin Dm0 (1:100), α–BEAF-32 (1:20), and α-HP1 (C1A9; 1:100; all obtained from Developmental Studies Hybridoma Bank); α-Polycomb (1:200; Santa Cruz Biotechnology, Inc.); and α–cleaved caspase-3 (1:200; Cell Signaling Technology). Secondary antibodies labeled with the fluorochromes FITC or Texas red were obtained from Jackson ImmunoResearch Laboratories, Inc. and used at 1:500–1:1,000.

S2 cell culture, transfection, and DsRNA treatment

Cells were maintained in insect media (HyClone SFX; Thermo Fisher Scientific) supplemented with penicillin/streptomycin at 25°C. Transfection of S2 cells was achieved using Lipofectin (Invitrogen). In brief, 1–3 µg of vector was combined with 15 µl Lipofectin in 1 ml SFX media and overlayed on 2×10^6 cells for 24 h. After 3–4 d, SFX media containing 300 µg/ml hygromycin (Invitrogen) was added to select stable lines. Expression was induced with 500 µM $CuSO_4^{2-} \cdot 5H_2O$ added to each flask 14–16 h before imaging. For DsRNA treatment, $\sim 10^6$ S2 cells were seeded in a 6-well plate and treated with 15 µg CP190 DsRNA daily for ≥4 d (Butcher et al., 2004) and prepared for imaging as described in Stress treatment and immunostaining (Rogers and Rogers, 2008). Knockdown levels were monitored by lysing $\sim 10^7$ S2 cells on ice in 100 µl radioimmunoprecipitation assay buffer supplemented with protease inhibitor (Roche). 12 µg of lysate was resolved in a 7.5% acrylamide gel, wet transferred at 4°C overnight (10 V), and probed with α-CP190 (1:1,500) and α-Su(Hw) (1:1,000).

Stress treatment and immunostaining

S2 cells 3–5 d after subculture were allowed to adhere to a poly-L-lysine coverslip for 30 min in a covered 35-mm cell culture dish. To induce osmostress, media were removed and quickly replaced with fresh SFX media supplemented with the indicated concentration of osmolyte (from a 5-M stock). Controls were kept in conditioned media. Cells were stressed for 20 min and then immunostained as previously described (Rogers and Rogers 2008). In brief, cells were fixed with 4% PFA for 10 min at RT, rinsed 3× with PBS, permeabilized with 0.2% Triton X-100 for 5 min, and blocked with 3% nonfat milk for 10 min at RT. Primary antibodies were diluted in 3% nonfat milk, and coverslips were incubated for 1 h at RT in a humidified chamber followed by a 3× wash with PBS/0.1% Triton X-100 for 10 min each. Secondary antibodies were then diluted in 3% nonfat milk and incubated for 1 h at RT, and coverslips were washed as described. 0.5 µg/ml DAPI was added to counterstain DNA, rinsed 2× with H_2O, and mounted in Vectashield. For larval and ovary tissue, Oregon-R third instar larvae and adult females were quickly dissected in SFX media and transferred to 0.5-ml tubes containing 500 µl SFX media supplemented with 0.5% BSA and the required concentration of osmolyte. Controls were treated similarly, with the exception that the osmolyte was excluded. Tubes were rotated at RT for 20 min to induce osmostress and immunostained as previously described (de Saint Phalle, 2004) with the following adjustments: tissues were fixed for 25 min in 0.5% Triton X-100/4% PFA and block permeabilized in 0.5% Triton X-100/1% BSA for ≥2 h with rotation to speed fixation and increase antigen accessibility in salivary glands.

For heat shock, 1 ml of ∼50% confluent S2 cells was seeded onto a coverslip containing poly-L-lysine in a 35-mm cell culture dish and allowed to adhere overnight at 25°C. Dishes were then placed in a 37°C H_2O bath such that the level of water outside the dish and media inside the dish were equal and incubated for either 20 or 60 min and then fixed immediately for immunostaining. To induce chromatin condensation independently of osmotic stress, S2 cells adhered to coverslips were treated with 50 mM Na azide in media for 20 min at RT.

Buffer/dissection condition stress test

To test the effects of dissection buffer/conditions on insulator body formation, third instar larvae were dissected in shallow depression slides containing 100 µl of either HyClone SFX insect media, PBS (137 mM NaCl, 2.7 mM KCl, 10 mM Na_2HPO_4, and 1.8 mM KH_2PO_4, pH 7.4), or *Drosophila* Ringer's solution (3 mM $CaCl_2 \cdot H_2O$, 182 mM KCl, 46 mM NaCl, and 10 mM Tris-HCl, pH 7.2). Dissections were performed in ∼5 min and either fixed immediately with 4% PFA/0.3% Triton X-100/PBS or left to incubate on the benchtop under nonhumidifying conditions for 30 min before fixation. Subsequent immunostaining was then performed as described. For S2 cells, 100 µl of ∼50% confluent S2 cells were pelleted at 500 rpm and resuspended in 100 µl of either PBS or Ringer's solution and distributed evenly over a 22 × 22–mm poly-L-lysine coverslip and allowed to adhere for 30 min in a 35-mm cell culture dish with the lid removed before fixation. Controls were kept covered in conditioned media and allowed to adhere for the same amount of time. Cells were then stained as described.

Detergent permeabilization before osmostress

S2 cells were allowed to adhere to concanavalin A–treated coverslips in conditioned media for 30 min at RT. The media were then aspirated, and Triton X-100 diluted to 0.2% in conditioned media was then quickly overlaid on the cells and incubated for 5 min at RT. Controls were treated with conditioned media without detergent. After aspiration, 250 mM NaCl + media was overlaid on the cells, treated for 15 min at RT, and then fixed and stained as described.

Nuclear halos

Nuclear halos from S2 were prepared as previously described (Byrd and Corces, 2003; Pathak et al., 2007) with the following exceptions. First, S2 cells were allowed to attach to poly-L-lysine coverslips for 45 min at RT. Cells were then either treated with media containing 250 mM NaCl or left untreated for 20 min followed by extraction with 2 M NaCl (2 M NaCl, 5 mM Hepes, pH 7.5, 2 mM KCl, 2 mM EDTA, 0.05% Triton X-100, and protease inhibitor) for 5 min at RT. Slips were briefly rinsed 3× in PBS and then fixed with 4% PFA for 10 min. Subsequent immunostaining was performed as described in Stress treatment and immunostaining.

Microscopy and live imaging

All immunostaining and live-imaging experiments were performed on a wide-field epifluorescent microscope (DM6000 B; Leica) equipped with HCX Plan Apochromat (Leica) 63×/1.4 NA and 100×/1.35 NA oil immersion objectives and a charge-coupled device camera (ORCA-ER; Hamamatsu Photonics). SimplePCI (v6.6; Hamamatsu Photonics) was used for image acquisition. Image processing of raw z stacks was performed using 3D Deconvolution Algorithm (AutoQuant) using an adaptive (blind) point spread function implemented into Deblur (v2.3.2) software (Leica). Final brightness/contrast adjustments after deconvolution were performed using ImageJ (v1.47b; National Institutes of Health). For live-imaging experiments, S2 cells were placed into an imaging chamber (µ-Slide upright$^{0.8}$; ibidi) and allowed to adhere to the top of the chamber for 20 min. A perfusion system using gravity flow allowed for the gradual addition of SFX media containing osmolyte to induce osmostress. All experiments were performed at RT (∼23°C). Lamp output (100 W) for each channel was reduced to 10%, and experiments were kept under 2 h to minimize photobleaching, toxicity, and focus drift. For salivary glands and imaginal discs, tissues were dissected in SFX media and anchored to a coverslip containing poly-L-lysine. This coverslip was then oriented tissue-side down over the top of a depression slide filled with SFX media, leaving one edge open to allow for gas exchange and access to the media pool. A thin layer of nail polish applied to one corner prevented movement of the coverslip during imaging. Salt treatment and recovery were performed by carefully removing the existing media in the depression slide with a pipette and slowly adding back the media of interest. Z stacks were taken at the indicated time intervals, and each raw stack was then processed using AutoQuant software as described for fixed samples and assembled using ImageJ. Final brightness/contrast adjustments and further image analysis were also performed using ImageJ and the plugins MTrackJ (Meijering et al., 2012) and Intensity Correlation Analysis (Li et al., 2004). DAPI, FITC, and Texas red fluorochromes were used for fixed samples, whereas EGFP and mCherry were used for live imaging.

FRAP analysis

FRAP was performed using the spinning-disc confocal platform (Marianas; Intelligent Imaging Innovations) consisting of an inverted microscope (Axio Observer; Carl Zeiss) outfitted with a spinning disc (CSU-X1; Carl Zeiss), an electron multiplying charge-coupled device camera (Evolve 512; Photometrics), high speed point scanner (Vector Laboratories), and a Plan Apochromat 100×/1.4 NA oil objective. S2 cells expressing Su(Hw)-EGFP

were stressed with 250 mM NaCl + SFX media, and cells expressing low amounts of transfected protein were imaged at RT (~23°C). Roughly three bodies per cell were bleached simultaneously using a 488-nm laser set to 100% (50 mW), frames were acquired every 250 ms, and recoveries were recorded and monitored in real time using SlideBook 5.0 software (Intelligent Imaging Innovations) and terminated once the curve plateaued. ImageJ was used to extract intensity measurements from each region of interest. Raw intensities were corrected for photobleaching and subtracted from background as previously described (Zheng et al., 2011) and normalized, with the final prebleach frame intensity taken to be 1. Recovery curves were plotted and fitted to a one-phase association exponential function using Prism 6 software (GraphPad Software). The mobile fraction and half-time of recovery were calculated from this curve as previously described (Reits and Neefjes, 2001).

ChIP

10^7 S2 cells were used for ChIP. Osmolyte stress was performed in 1.5-ml tubes containing 250 mM NaCl in SFX media and rotated for 20 min at RT. Controls were kept in the same conditioned media. For recovery treatments, cells were stressed with osmolyte for 20 min, pelleted at 2,500 *g* for 2.5 min, and then gently resuspended in 1 ml of fresh SFX media and rotated for 2.5 min at RT. ChIP was performed essentially as previously described (Wu et al., 2003) as follows: cross-linking was performed by adding 16% PFA to a final concentration of 1%, and tubes were rotated for 10 min at RT. Cells were then pelleted and resuspended in 1% SDS lysis buffer (1% SDS, 10 mM EDTA, 50 mM Tris-HCl, pH 8.1, and protease inhibitor) and placed on ice for 10 min. Chromatin was sheared to a mean size of 500 bp using a sonication device (Bioruptor; Diagenode) coupled to a continual flow 4°C H_2O bath using the following parameters: high power and 30× cycles of 30 s on and 30 s off. Insoluble debris were pelleted, and the supernatant was diluted 10-fold in immunoprecipitation buffer (0.01% SDS, 1.1% Triton X-100, 1.2 mM EDTA, 16.7 mM Tris-HCl, pH 8.1, 16.7 mM NaCl, and protease inhibitor). Diluted chromatin extracts were precleared using 100 µl protein A–agarose beads (Invitrogen) for 30 min at 4°C. 300 µl of this solution was used for each pull-down, using 5 µl α-Su(Hw) (previously ChIP validated; Wallace et al., 2010) overnight at 4°C; mock controls were also included. Antibody–antigen complexes were recovered using 35 µl protein A–agarose beads for 2 h at 4°C, and the beads were harvested by centrifugation and serially washed for 20 min each at 4°C with 1 ml of the following wash buffers: low salt wash (0.1% SDS, 1% Triton X-100, 2 mM EDTA, 20 mM Tris-HCl, pH 8.1, and 150 mM NaCl), high salt wash (0.1% SDS, 1% Triton X-100, 2 mM EDTA, 20 mM Tris-HCl, pH 8.1, and 500 mM NaCl), lithium wash (0.25 M LiCl, 1% NP-40, 1% Na deoxycholate, 1 mM EDTA, and 10 mM Tris-HCl, pH 8.1), and TE (Tris-EDTA). Beads were then resuspended in 1 ml TE and transferred to a new tube. Antibody–antigen complexes were eluted from the beads using 500 µl elution buffer (1% SDS and 0.1 M $NaHCO_3$) and incubated at RT for 30 min. 10% input controls were also diluted in elution buffer to final volume of 300 µl, and 20 µl of 5-M NaCl was added to all samples and placed at 65°C overnight to reverse formaldehyde cross-links. 2 µl of 10-mg/ml proteinase K was then added and incubated 1 h at 65°C. Solutions were extracted once with an equal volume of phenol/chloroform/isoamyl alcohol, EtOH precipitated, washed, and resuspended in 25 µl nuclease-free H_2O.

Real-time PCR quantification of ChIP samples

Runs were performed on a cycler (iQ5; Bio-Rad Laboratories) using SYBR Green Supermix (iQ; Bio-Rad Laboratories). Three biological replicates for each treatment (control, osmolyte stress, and recovery) were included in addition to three technical replicates for each. Primer sets for each insulator were designed based on ChIP-chip data (Nègre et al., 2010), and all gave 98–101% amplification efficiencies. Rp49 was used as a negative control region. Data were normalized using the percent input method, and a paired Student's *t* test was used to assess statistical significance.

Quantitative 3C

3C was performed in ~10^8 S2 cells treated with or without 250 mM NaCl for 5 min at RT as previously described (Comet et al., 2011) with the following adjustments: cells were cross-linked for 10 min at RT on a rotating platform using 10 ml of a 1% PFA/SFX media solution, dounce homogenized (20 strokes) in nuclear preparation buffer on ice, and digested at 37°C at 400 rpm overnight with 1,500 U EcoRI (New England Biolabs, Inc.). 100 U T4 ligase (New England Biolabs, Inc.) was used for ligation, which was performed for 4 h at RT with gentle shaking. Cross-links were reversed at 65°C at 400 rpm overnight, incubated with 25 µl of 10-mg/ml Proteinase K at 56°C for 4 h at 400 rpm, and extracted with a single round of phenol/chloroform/isoamyl alcohol. DNA was EtOH precipitated and resuspended in 50–75 µl H_2O. Concentrations were determined using a fluorometer, and all samples were diluted to ~50 ng/µl. Sample purity was assessed via quantitative PCR (qPCR) SYBR green quantification using a 10-fold serial dilution of each template and amplifying with RP49 primers; samples showing >110% amplification efficiencies were repurified with phenol/chloroform. Digestion efficiency calculations and data analysis/normalization were performed as previously described (Hagège et al., 2007). Two minimally overlapping bacterial artificial chromosome clones used for normalization were obtained from the Children's Hospital Oakland Research Institute (BACR48A11 and BACR28012). A Student's paired *t* test was used to assess statistical significance based on three biological replicates per treatment.

RNA extraction, cDNA synthesis, RT-PCR, and qPCR

Oregon-R, *yw, dMEKK1^{UR36}*, and *bsk (JNK)-RNAi ± UAS-Dcr-2; eng-Gal4* wing discs (approximately six pairs) were dissected in triplicate in SFX media and RNA extracted using 300 µl TRIZOL (Invitrogen). Entire *p38b$^{\Delta 45}$* and *p38b$^{\Delta 25}$; p38a^{del}* third instar larvae (four to six) were homogenized and similarly extracted with 300 µl TRIZOL. Samples were treated with TURBO-free DNase (Ambion), and 500 ng RNA was used for cDNA synthesis using the cDNA synthesis kit with oligo dT primers (iScript; Bio-Rad Laboratories). RT-PCR/qPCR runs were performed on an iQ5 cycler using iQ SYBR green supermix using 1 µl cDNA. 10 µl of each representative genotype was resolved on a 1.5% agarose gel and imaged using a gel documentation system (EpiChemi^3; UVP). To measure JNK RNAi knockdown, fold enrichment was calculated by comparing gene-specific cycle threshold (C_t) values to Rp49 C_t values following the $\Delta\Delta C_t$ method. A paired Student's *t* test was used to assess statistical significance based on three biological replicates per treatment.

Western blotting

10^7 S2 cells were lysed on ice in 100 µl radioimmunoprecipitation assay buffer supplemented with protease inhibitor and the SUMO isopeptidase inhibitors *N*-ethylmaleimide (80 mM; Sigma-Aldrich) and iodoacetamide (0.2 mM; Acros Organics). For stress/recovery experiments, S2 cells in media were rotated in 1.5-ml tubes at RT with or without 250 mM NaCl in SFX media for 20 min. For recovery, stressed cells were pelleted at 2,500 *g* for 2 min and gently resuspended in fresh SFX media for the indicated amount of time before being lysed. 12 µg lysate was resolved in a 7.5% acrylamide gel, wet transferred at 4°C overnight (10 V), and probed with α-CP190 (1:1,500), α-Su(Hw) (1:1,000), or α-Mod(mdg4)67.2 (1:1,000).

Online supplemental material

Fig. S1 verifies that insulator body formation is triggered by osmotic stress and rules out heat shock as a possible inducer. Fig. S2 confirms that the tagged Su(Hw)::EGFP accurately reproduces the behavior of the endogenous protein and that BEAF-32 donut formation is not an antibody artifact. Fig. S3 provides evidence that DsRNA-mediated knockdown of CP190 in S2 cells impairs the ability of Mod(mdg4) to enter bodies, while also verifying that *su(Hw)* mutations do not prevent Mod or CP190 from forming bodies in tissue. Fig. S4 confirms the mutant alleles for *dMekk1*, *p38a*, and *p38b* by RT-PCR, while qPCR verifies reduction of *JNK* in wing discs. Fig. S5 provides evidence that insulator bodies are also evident in tissues undergoing cell death and that body formation is not dependent on chromatin condensation nor does it lead to alterations in gene expression. Video 1 shows Su(Hw)/BEAF-32 insulator body formation in S2 cells after osmostress induction. Video 2 reveals that insulator body formation is rapidly reversible in larval salivary glands during recovery in isotonic media. Video 3 shows that multiple rounds of rapid insulator body assembly and disassembly are observable in diploid tissues. Video 4 provides a close up of the initial body formation in these tissues. Online supplemental material is available at http://www.jcb.org/cgi/content/full/jcb.201304181/DC1. Additional data are available in the JCB DataViewer at http://dx.doi.org/10.1083/jcb.201304181.dv.

We thank Victor Corces, Tom Dockendorff, Bruce McKee, Hyung Don Ryoo, Alysia Vrailas-Mortimer, the Bloomington Stock Center, Transgenic RNAi Project at Harvard Medical School (National Institutes of Health/National Institute of General Medical Sciences grant R01-GM084947), the Developmental Studies Hybridoma Bank (National Institute of Child Health and Human Development/University of Iowa), and Andreas Nebenführ for fly stocks, antibodies, and plasmids.

We also thank the Biochemistry and Cellular and Molecular Biology Department, the College of Arts and Sciences, and Office of Research at the University of Tennessee for support in addition to the US Public Health Service Award (GM78132-2) from the National Institutes of Health and from National Science Foundation (0616081) to M. Labrador. J. Barrios was a Summer Research Experiences for Undergraduates fellow (National Science Foundation Award DBI-1156744 to the Biochemistry and Cellular and Molecular Biology Department). T. Schoborg and R. Rickels are recipients of Graduate Research Fellowships from the National Science Foundation.

Submitted: 26 April 2013
Accepted: 17 June 2013

References

Alkema, M.J., M. Bronk, E. Verhoeven, A. Otte, L.J. van 't Veer, A. Berns, and M. van Lohuizen. 1997. Identification of Bmi1-interacting proteins as constituents of a multimeric mammalian polycomb complex. *Genes Dev.* 11:226–240. http://dx.doi.org/10.1101/gad.11.2.226

Bantignies, F., V. Roure, I. Comet, B. Leblanc, B. Schuettengruber, J. Bonnet, V. Tixier, A. Mas, and G. Cavalli. 2011. Polycomb-dependent regulatory contacts between distant Hox loci in *Drosophila. Cell*. 144:214–226. http://dx.doi.org/10.1016/j.cell.2010.12.026

Biamonti, G., and C. Vourc'h. 2010. Nuclear stress bodies. *Cold Spring Harb. Perspect. Biol.* 2:a000695. http://dx.doi.org/10.1101/cshperspect.a000695

Burg, M.B., J.D. Ferraris, and N.I. Dmitrieva. 2007. Cellular response to hyperosmotic stresses. *Physiol. Rev.* 87:1441–1474. http://dx.doi.org/10.1152/physrev.00056.2006

Bushey, A.M., E. Ramos, and V.G. Corces. 2009. Three subclasses of a *Drosophila* insulator show distinct and cell type-specific genomic distributions. *Genes Dev.* 23:1338–1350. http://dx.doi.org/10.1101/gad.1798209

Butcher, R.D.J., S. Chodagam, R. Basto, J.G. Wakefield, D.S. Henderson, J.W. Raff, and W.G.F. Whitfield. 2004. The *Drosophila* centrosome-associated protein CP190 is essential for viability but not for cell division. *J. Cell Sci.* 117:1191–1199. http://dx.doi.org/10.1242/jcs.00979

Byrd, K., and V.G. Corces. 2003. Visualization of chromatin domains created by the *gypsy* insulator of *Drosophila*. *J. Cell Biol.* 162:565–574. http://dx.doi.org/10.1083/jcb.200305013

Capelson, M., and V.G. Corces. 2005. The ubiquitin ligase dTopors directs the nuclear organization of a chromatin insulator. *Mol. Cell*. 20:105–116. http://dx.doi.org/10.1016/j.molcel.2005.08.031

Capelson, M., and V.G. Corces. 2006. SUMO conjugation attenuates the activity of the gypsy chromatin insulator. *EMBO J.* 25:1906–1914. http://dx.doi.org/10.1038/sj.emboj.7601068

Comet, I., B. Schuettengruber, T. Sexton, and G. Cavalli. 2011. A chromatin insulator driving three-dimensional Polycomb response element (PRE) contacts and Polycomb association with the chromatin fiber. *Proc. Natl. Acad. Sci. USA*. 108:2294–2299. http://dx.doi.org/10.1073/pnas.1002059108

Craig, C.R., J.L. Fink, Y. Yagi, Y.T. Ip, and R.L. Cagan. 2004. A *Drosophila* p38 orthologue is required for environmental stress responses. *EMBO Rep.* 5:1058–1063. http://dx.doi.org/10.1038/sj.embor.7400282

Cuddapah, S., R. Jothi, D.E. Schones, T.Y. Roh, K. Cui, and K. Zhao. 2009. Global analysis of the insulator binding protein CTCF in chromatin barrier regions reveals demarcation of active and repressive domains. *Genome Res.* 19:24–32. http://dx.doi.org/10.1101/gr.082800.108

de Saint Phalle, B. 2004. Immunostaining of whole-mount imaginal discs. *Methods Mol. Biol.* 247:373–387.

Fujioka, M., X. Wu, and J.B. Jaynes. 2009. A chromatin insulator mediates transgene homing and very long-range enhancer-promoter communication. *Development*. 136:3077–3087. http://dx.doi.org/10.1242/dev.036467

Gerasimova, T.I., and V.G. Corces. 1998. Polycomb and trithorax group proteins mediate the function of a chromatin insulator. *Cell*. 92:511–521. http://dx.doi.org/10.1016/S0092-8674(00)80944-7

Gerasimova, T.I., K. Byrd, and V.G. Corces. 2000. A chromatin insulator determines the nuclear localization of DNA. *Mol. Cell*. 6:1025–1035. http://dx.doi.org/10.1016/S1097-2765(00)00101-5

Gerasimova, T.I., E.P. Lei, A.M. Bushey, and V.G. Corces. 2007. Coordinated control of dCTCF and gypsy chromatin insulators in *Drosophila*. *Mol. Cell*. 28:761–772. http://dx.doi.org/10.1016/j.molcel.2007.09.024

Ghosh, D., T.I. Gerasimova, and V.G. Corces. 2001. Interactions between the Su(Hw) and Mod(mdg4) proteins required for gypsy insulator function. *EMBO J.* 20:2518–2527. http://dx.doi.org/10.1093/emboj/20.10.2518

Golovnin, A., L. Melnikova, I. Volkov, M. Kostuchenko, A.V. Galkin, and P. Georgiev. 2008. 'Insulator bodies' are aggregates of proteins but not of insulators. *EMBO Rep.* 9:440–445. http://dx.doi.org/10.1038/embor.2008.32

Golovnin, A., I. Volkov, and P. Georgiev. 2012. SUMO conjugation is required for the assembly of *Drosophila* Su(Hw) and Mod(mdg4) into insulator bodies that facilitate insulator complex formation. *J. Cell Sci.* 125:2064–2074. http://dx.doi.org/10.1242/jcs.100172

Hagège, H., P. Klous, C. Braem, E. Splinter, J. Dekker, G. Cathala, W. de Laat, and T. Forné. 2007. Quantitative analysis of chromosome conformation capture assays (3C-qPCR). *Nat. Protoc.* 2:1722–1733. http://dx.doi.org/10.1038/nprot.2007.243

Han, S.J., K.Y. Choi, P.T. Brey, and W.J. Lee. 1998. Molecular cloning and characterization of a *Drosophila* p38 mitogen-activated protein kinase. *J. Biol. Chem.* 273:369–374. http://dx.doi.org/10.1074/jbc.273.1.369

Hou, C., L. Li, Z.S. Qin, and V.G. Corces. 2012. Gene density, transcription, and insulators contribute to the partition of the *Drosophila* genome into physical domains. *Mol. Cell*. 48:471–484. http://dx.doi.org/10.1016/j.molcel.2012.08.031

Inoue, H., M. Tateno, K. Fujimura-Kamada, G. Takaesu, T. Adachi-Yamada, J. Ninomiya-Tsuji, K. Irie, Y. Nishida, and K. Matsumoto. 2001. A *Drosophila* MAPKKK, D-MEKK1, mediates stress responses through activation of p38 MAPK. *EMBO J.* 20:5421–5430. http://dx.doi.org/10.1093/emboj/20.19.5421

Krivega, I., and A. Dean. 2012. Enhancer and promoter interactions-long distance calls. *Curr. Opin. Genet. Dev.* 22:79–85. http://dx.doi.org/10.1016/j.gde.2011.11.001

Labrador, M., and V.G. Corces. 2002. Setting the boundaries of chromatin domains and nuclear organization. *Cell*. 111:151–154. http://dx.doi.org/10.1016/S0092-8674(02)01004-8

Lafarga, M., M.T. Berciano, E. Pena, I. Mayo, J.G. Castaño, D. Bohmann, J.P. Rodrigues, J.P. Tavanez, and M. Carmo-Fonseca. 2002. Clastosome: a subtype of nuclear body enriched in 19S and 20S proteasomes, ubiquitin, and protein substrates of proteasome. *Mol. Biol. Cell*. 13:2771–2782. http://dx.doi.org/10.1091/mbc.E02-03-0122

Lei, E.P., and V.G. Corces. 2006. RNA interference machinery influences the nuclear organization of a chromatin insulator. *Nat. Genet.* 38:936–941. http://dx.doi.org/10.1038/ng1850

Li, Q., A. Lau, T.J. Morris, L. Guo, C.B. Fordyce, and E.F. Stanley. 2004. A syntaxin 1, Galpha(o), and N-type calcium channel complex at a presynaptic nerve terminal: analysis by quantitative immunocolocalization. *J. Neurosci.* 24:4070–4081. http://dx.doi.org/10.1523/JNEUROSCI.0346-04.2004

Meijering, E.O.D., O. Dzyubachyk, and I. Smal. 2012. Methods for cell and particle tracking. *Methods Enzymol.* 504:183–200. http://dx.doi.org/10.1016/B978-0-12-391857-4.00009-4

Messmer, S., A. Franke, and R. Paro. 1992. Analysis of the functional role of the Polycomb chromo domain in *Drosophila melanogaster. Genes Dev.* 6:1241–1254. http://dx.doi.org/10.1101/gad.6.7.1241

Mozer, B.A. 2001. Dominant Drop mutants are gain-of-function alleles of the muscle segment homeobox gene (msh) whose overexpression leads to the arrest of eye development. *Dev. Biol.* 233:380–393. http://dx.doi.org/10.1006/dbio.2001.0229

Nègre, N., C.D. Brown, P.K. Shah, P. Kheradpour, C.A. Morrison, J.G. Henikoff, X. Feng, K. Ahmad, S. Russell, R.A. White, et al. 2010. A comprehensive map of insulator elements for the *Drosophila* genome. *PLoS Genet.* 6:e1000814. http://dx.doi.org/10.1371/journal.pgen.1000814

Oliver, D., B. Sheehan, H. South, O. Akbari, and C.Y. Pai. 2010. The chromosomal association/dissociation of the chromatin insulator protein Cp190 of *Drosophila melanogaster* is mediated by the BTB/POZ domain and two acidic regions. *BMC Cell Biol.* 11:101. http://dx.doi.org/10.1186/1471-2121-11-101

Pai, C.Y., E.P. Lei, D. Ghosh, and V.G. Corces. 2004. The centrosomal protein CP190 is a component of the gypsy chromatin insulator. *Mol. Cell*. 16:737–748. http://dx.doi.org/10.1016/j.molcel.2004.11.004

Pathak, R.U., N. Rangaraj, S. Kallappagoudar, K. Mishra, and R.K. Mishra. 2007. Boundary element-associated factor 32B connects chromatin domains to the nuclear matrix. *Mol. Cell. Biol.* 27:4796–4806. http://dx.doi.org/10.1128/MCB.00305-07

Ramos, E., E.A. Torre, A.M. Bushey, B.V. Gurudatta, and V.G. Corces. 2011. DNA topoisomerase II modulates insulator function in *Drosophila. PLoS ONE*. 6:e16562. http://dx.doi.org/10.1371/journal.pone.0016562

Reits, E.A.J., and J.J. Neefjes. 2001. From fixed to FRAP: measuring protein mobility and activity in living cells. *Nat. Cell Biol.* 3:E145–E147. http://dx.doi.org/10.1038/35078615

Richter, K., M. Nessling, and P. Lichter. 2008. Macromolecular crowding and its potential impact on nuclear function. *Biochim. Biophys. Acta*. 1783:2100–2107. http://dx.doi.org/10.1016/j.bbamcr.2008.07.017

Rogers, S.L., and G.C. Rogers. 2008. Culture of *Drosophila* S2 cells and their use for RNAi-mediated loss-of-function studies and immunofluorescence microscopy. *Nat. Protoc.* 3:606–611. http://dx.doi.org/10.1038/nprot.2008.18

Saito, H., and F. Posas. 2012. Response to hyperosmotic stress. *Genetics*. 192:289–318. http://dx.doi.org/10.1534/genetics.112.140863

Schoborg, T.A., and M. Labrador. 2010. The phylogenetic distribution of non-CTCF insulator proteins is limited to insects and reveals that BEAF-32 is *Drosophila* lineage specific. *J. Mol. Evol.* 70:74–84. http://dx.doi.org/10.1007/s00239-009-9310-x

Seong, K.H., D. Li, H. Shimizu, R. Nakamura, and S. Ishii. 2011. Inheritance of stress-induced, ATF-2-dependent epigenetic change. *Cell*. 145:1049–1061. http://dx.doi.org/10.1016/j.cell.2011.05.029

Sexton, T., E. Yaffe, E. Kenigsberg, F. Bantignies, B. Leblanc, M. Hoichman, H. Parrinello, A. Tanay, and G. Cavalli. 2012. Three-dimensional folding and functional organization principles of the *Drosophila* genome. *Cell*. 148:458–472. http://dx.doi.org/10.1016/j.cell.2012.01.010

Van Bortle, K., and V.G. Corces. 2012. Nuclear organization and genome function. *Annu. Rev. Cell Dev. Biol.* 28:163–187. http://dx.doi.org/10.1146/annurev-cellbio-101011-155824

Veraksa, A., A. Bauer, and S. Artavanis-Tsakonas. 2005. Analyzing protein complexes in *Drosophila* with tandem affinity purification-mass spectrometry. *Dev. Dyn.* 232:827–834. http://dx.doi.org/10.1002/dvdy.20272

Vermaak, D., and H.S. Malik. 2009. Multiple roles for heterochromatin protein 1 genes in *Drosophila*. *Annu. Rev. Genet.* 43:467–492. http://dx.doi.org/10.1146/annurev-genet-102108-134802

Vrailas-Mortimer, A., T. del Rivero, S. Mukherjee, S. Nag, A. Gaitanidis, D. Kadas, C. Consoulas, A. Duttaroy, and S. Sanyal. 2011. A muscle-specific p38 MAPK/Mef2/MnSOD pathway regulates stress, motor function, and life span in *Drosophila*. *Dev. Cell*. 21:783–795. http://dx.doi.org/10.1016/j.devcel.2011.09.002

Wallace, H.A., M.P. Plata, H.J. Kang, M. Ross, and M. Labrador. 2010. Chromatin insulators specifically associate with different levels of higher-order chromatin organization in *Drosophila*. *Chromosoma*. 119:177–194. http://dx.doi.org/10.1007/s00412-009-0246-0

Wood, A.M., K. Van Bortle, E. Ramos, N. Takenaka, M. Rohrbaugh, B.C. Jones, K.C. Jones, and V.G. Corces. 2011. Regulation of chromatin organization and inducible gene expression by a *Drosophila* insulator. *Mol. Cell*. 44:29–38. http://dx.doi.org/10.1016/j.molcel.2011.07.035

Wu, C.-H., Y. Yamaguchi, L.R. Benjamin, M. Horvat-Gordon, J. Washinsky, E. Enerly, J. Larsson, A. Lambertsson, H. Handa, and D. Gilmour. 2003. NELF and DSIF cause promoter proximal pausing on the hsp70 promoter in *Drosophila*. *Genes Dev.* 17:1402–1414. http://dx.doi.org/10.1101/gad.1091403

Xu, Q., M. Li, J. Adams, and H.N. Cai. 2004. Nuclear location of a chromatin insulator in *Drosophila melanogaster*. *J. Cell Sci.* 117:1025–1032. http://dx.doi.org/10.1242/jcs.00964

Yang, J., and V.G. Corces. 2012. Insulators, long-range interactions, and genome function. *Curr. Opin. Genet. Dev.* 22:86–92. http://dx.doi.org/10.1016/j.gde.2011.12.007

Yujiri, T., G.R. Fanger, T.P. Garrington, T.K. Schlesinger, S. Gibson, and G.L. Johnson. 1999. MEK kinase 1 (MEKK1) transduces c-Jun NH2-terminal kinase activation in response to changes in the microtubule cytoskeleton. *J. Biol. Chem.* 274:12605–12610. http://dx.doi.org/10.1074/jbc.274.18.12605

Zheng, C.-Y., R.S. Petralia, Y.-X. Wang, and B. Kachar. 2011. Fluorescence recovery after photobleaching (FRAP) of fluorescence tagged proteins in dendritic spines of cultured hippocampal neurons. *J. Vis. Exp.* 50:2568.

Zhong, S., P. Salomoni, and P.P. Pandolfi. 2000. The transcriptional role of PML and the nuclear body. *Nat. Cell Biol.* 2:E85–E90. http://dx.doi.org/10.1038/35010583